The Methanol-to-Olefins Reactions: the Influence of Water Studied by in situ Spectroscopy

Laurens Mandemaker

Daily Supervisor: Javier Ruiz-Martinez
First Examiner: Bert M. Weckhuysen
Second Examiner: Pieter C. A. Bruijnincx

Inorganic Chemistry and Catalysis
Faculty of science
Debye Institute for Nanomaterials Science

24 – February - 2016

Abstract

Operando UV-Vis has been used and analyzed to elaborate on the influence of water on the methanol-to-olefins reaction catalyzed by H-SAPO-34. It was shown that methanol concentration, not influenced by the nature of diluent, influences the catalytic performance. A lower methanol concentration gave rise to a higher total active time, a higher olefin yield and improved light olefin selectivity. Deactivation rates decreased and the contribution of active species was larger. This could be explained by an increased diffusion of methanol into the catalyst particles, giving rise to a higher amount of total species in the spent catalyst.

When the diluent was changed from only helium to helium + water (at different ratios) the effect of water was observed. Water was shown to have no influence on the product selectivity and no clear effect on the active period or reaction time. However, the contribution of active species and the total olefin yield increased. The amount of deactivated species present in the spent catalysts was similar for all methanol / water ratios. Using NNMF analysis, it became clear water influences the reactivity of the reagent / product feed with the active species. A propylene feeding experiment confirms this. The lower reactivity explains a decreased rate of formation for deactivating species and the higher olefin yield. The slower formation of active and deactivating species together with the higher contribution of active species at their maxima implies the reactivity of the reagent / product feed is lowered due to competitive adsorption with water.

Contents

Chapter 1 - Introduction

1.1 Methanol-to-Olefins

In a world with decreasing quantity of fossil fuels, alternative feedstocks are deployed as possible alternatives for chemical processes. One of these chemical processes is the formation of light olefins (ethylene & propylene). Light olefins are of great importance in the petrochemical branch because of their high energy density and easy transportability. In the consumers good market they play an essential role in the formation of polymers. [1] For decades light olefins are obtained by the steam cracking of natural gas liquids (NGL), naphtha or other light fractions of petroleum, all obtained from crude oil. [2], [3] Crude oil is not only diminishing; its contribution on the greenhouse effect has created great interest in alternative ways to obtain light olefins. With the synthesis of H-ZSM5 in the early 1970s and the first and second oil crisis in 1973 and 1979, respectively, followed by an extensive development program, a market was born for Methanol-to-Gasoline industry. [4] It was the discovery of H-SAPO-34 by researchers at Union Carbide (now UOP) that significantly improved the selectivity to light olefins and lead to the Methanol-to-Olefins (MTO) industry. In the nineties UOP and Norsk Hydro (now INEOS) developed an industrial based MTO process applying a low-pressure fluidized-bed reactor. Combining this process with an olefin cracking process (OCP), developed by Total Petrochemicals and UOP, ethylene/propylene selectivity were increased (see Figure 1). In 2009 a semi-commercial demonstration unit, processing up to 10 tons per day of methanol feed, was brought on-stream in Belgium, and in 2011 the construction of a 295 kt/y plant in China was announced. [1]

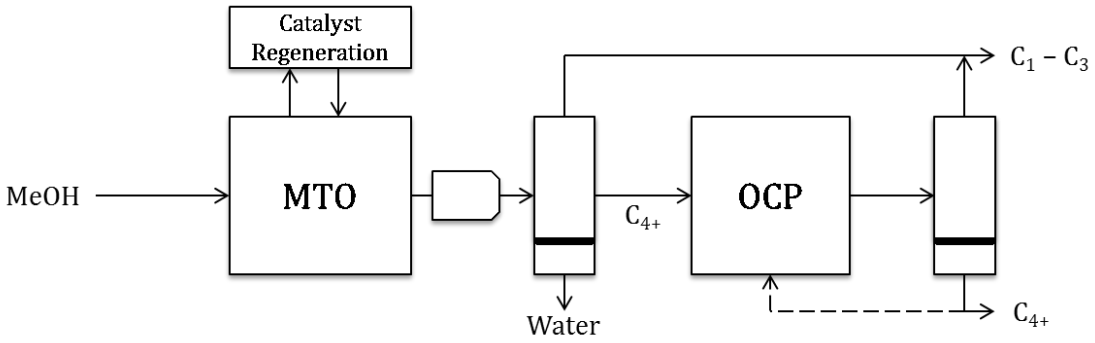

Figure 1. Schematic INEOS MTO fluidized-bed process (SAPO-34) combined with UOP/Total OCP olefin cracking process, reproduced from ref [1]

The production of methanol from synthesis gas using existing and proved technologies lays the foundation of MTO research. [3] Synthesis gas, or syngas, consists of mainly CO and H_2 and is obtained by the gasification of 'natural feedstocks' like natural gas, biomass and coal (see Figure 2). Therefore the combined processes of syngas-to-methanol and methanol-to-olefins make a 'green' alternative for the production of light olefins, if green natural feedstocks are used.

Figure 2. Oil alternative feedstocks: natural gas, biomass & coal (respectively)

1.2 Catalysts

Zeolites and zeotypes are the catalysts used for industrial methanol-to-hydrocarbon (MTH) processes. Their Brønsted acidity and shape selectivity makes them great candidates, also considering their low cost, high chemical and thermal stability and easy production. Besides, the wide variety of zeolites and zeotypes and possible modifications make a broad range of different product diversity when looking at MTH-reactions.[1], [5], [6]

1.2.1 Acidity

Zeolites are aluminosilicates with highly ordered structures and micro- and mesoporosity. Their primary structure consists of TO_4 tetrahedra sharing the edges, with an oxygen atom in each corner and a silica or alumina atom in the center. The micropores are formed by spatial and regular arrangement of the tetrahedral units. [7] When a silicon atom is replaced by an aluminum one, a negative charge is introduced into the lattice. To compensate this negative charge, positive counter ions are needed. In nature, these ions are mostly alkali-metal ions (like sodium or potassium) or ammonium ions. When a proton is used to counter this negative charge, a Brønsted acid site is introduced (Figure 3). [8] The strength of the acid-site depends on several factors, such as the amount of aluminum next-nearest neighbors (and thus the Si/Al ratio) and the position of the active site in the structure.

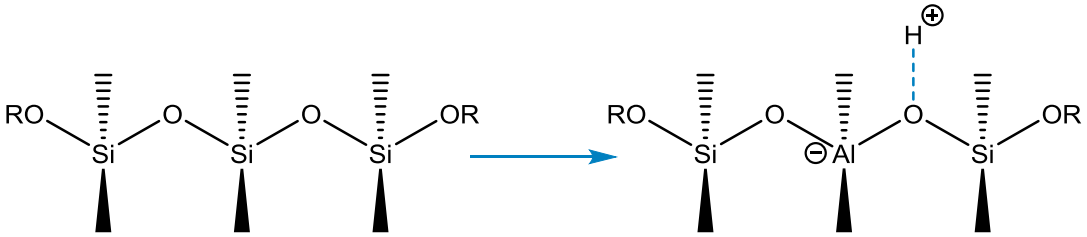

Figure 3. Schematic formation of a Brønsted acid site by Si/Al substitution and a proton counter ion

Zeotypes are zeolite-like materials with a similar crystalline structure but different chemical composition. Within these zeotypes are aluminophosphates, AlPOs. They possess the same framework types as zeolites but consist of alternating AlO_4 and PO_4 tetrahedra. When silicon is substituted into the framework a charge imbalance is created. So far, only phosphor is being replaced, since replacing aluminum doesn't introduce a negative charge. In the same fashion as in zeolites, a proton can balance the charge, creating a Brønsted acid (Figure 4). [9] It should be noted, however, that acid strength is most of the times weaker than in zeolites, making this catalyst more resistant to deactivation. [10]–[13]

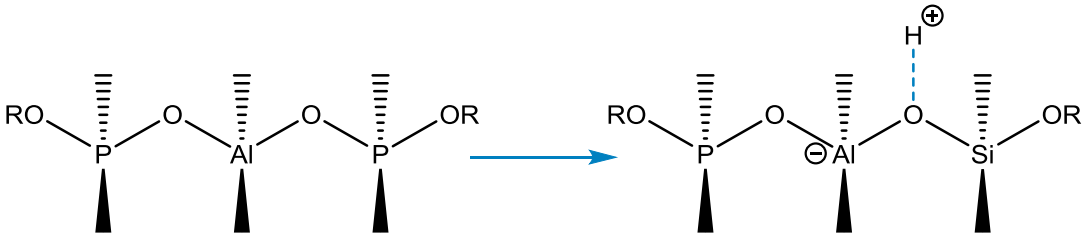

Figure 4. Schematic formation of Brønsted acid site by P/Si substitution and a proton counter ion in an AlPO

1.2.2 Shape Selectivity

Shape selectivity is another essential feature of zeolite materials. [14] Different types of shape selectivity can be observed: Reagent Shape Selectivity (RSS), Transition state Shape Selectivity (TSS) and Product Shape Selectivity (PSS). For the MTO/MTH-reactions, the most used zeolite or zeotype structures are chabazite (CHA) and MFI (Figure 5).

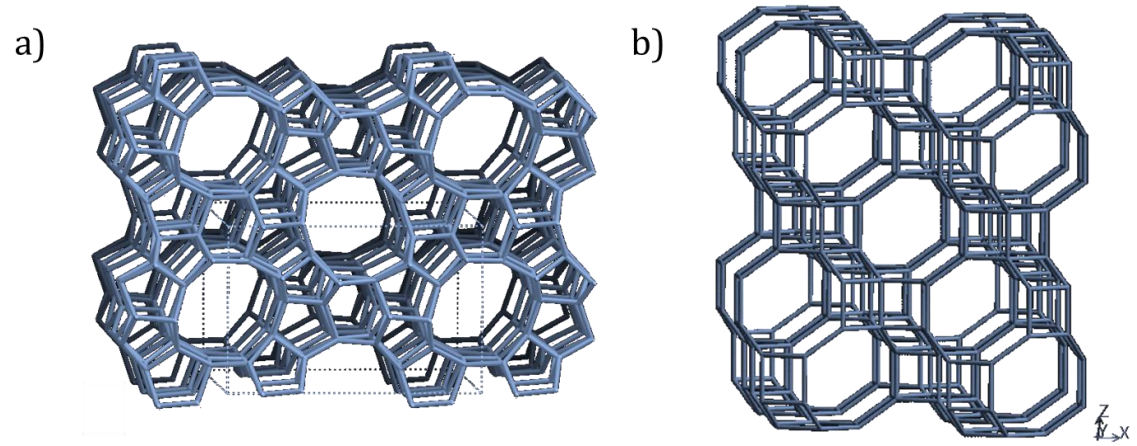

Figure 5. The MFI framework (left) as seen in ZSM-5 and the CHA framework (right) as seen in SAPO-34 and SSZ-13 [15]

When using both types of framework in MTO/MTH-reactions, PSS and TSS effects play a role. The small methanol is well able to diffuse into the catalyst so RSS could be applied in a combination of reactions and processes but is not applied in industry so far. Both structures have larger cavities so TSS doesn't seem to be of influence since molecules as large as pyrene are shown to form in the catalysts. [16] However, Corma et al. show that TSS plays a part in the MTO product selectivity since the product distribution of different samples was influenced by exposure of nano-SAPO-34 (CHA) to moisture for different amount of days, which would influence the acid strength only and not the diffusion of light olefins. [17] ZSM-5 is also known to stabilize olefins, therefore being more selective to propylene, which could be assumed to be a TSS effect since there's almost no hexamethylbenzene (HMB, active intermediate) present.

The CHA structured SAPO-34 and SSZ-13 have large cavities (0.65 nm x 1.0 nm) connected through narrow windows (0.42 nm x 0.37 nm). Although fairly large molecules can easily form in the cavities (including coke precursors), only small molecules can diffuse from cage to cage and eventually out of the catalyst as product. [16], [18] The MFI structure in ZSM-5 is based on 10-atom rings and the channels are wider (0.51 nm x 0.54 nm for the straight and 0.54 nm x 0.56 nm for the sinusoidal channels) than for CHA. This results in larger species being able to leave the catalyst, some species which have a crucial role in the MTO mechanism (as elaborated on later). [16], [18] As a result of these topological differences, different reaction products are observed as illustrated in the GC-MS analysis in Figure 6.

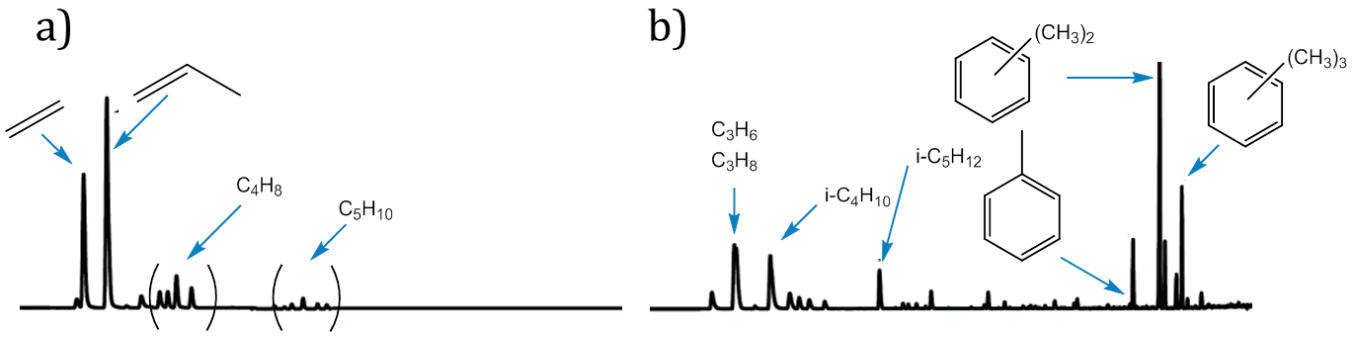

Figure 6. GC-MS chromatogram of A) H-SAPO-34 catalyzed MTO products and B) H-ZSM-5 catalyzed MTO products, reproduced from ref [16]

1.3 Mechanism

The catalytic mechanism for the MTO reaction has been a debate for years. Although mechanistic research on MTO started when it was discovered, there was no strong evidence for one single mechanism for many years. In general, the mechanism is believed to involve five phases. [16] First of all, there is the equilibrium between methanol and dimethyl ether (DME) and water. Second, there is an induction period on freshly activated catalyst beds that precedes a high yield of hydrocarbons formed from methanol and DME. The third and most debated phase is the formation of the first hydrocarbon product. Central is the formation of the first carbon-carbon (C-C) bond and how this bond is formed. According to Stöcker & colleagues, there have been at least 20 distinct mechanisms proposed for MTO catalysis. [12] The fourth phase is the conversion of light olefins to a mixture of other hydrocarbons. Although these conversions take place on acid sites in most zeolites/zeotypes, not all zeolites show the same range of products. For example, ZSM-5 product range is masked by products from secondary reactions, while SAPO-34s product range is limited (as also seen in Figure 6). The natures of these reactions are highly dependent on acid strength and catalyst topology [16], [19], and other factors like particle size and catalyst bed length will have an influence as well. At last, the fifth and final phase of methanol conversion is catalyst deactivation. This is mostly because of the formation of larger hydrocarbons which will eventually fill up the cavities and block the active sites, thus deactivating the catalyst.

1.3.1 The first C-C bond

The formation of the first carbon-carbon bond has been addressed by Song & colleagues and has been the central focus of MTO studies for many years. [20] Most MTO mechanisms found are named after a distinctive proposed intermediate. In the 1970s, Clarence Chang and Tony Silvestri of Mobil Research & Development did research on ZSM-5 to make high-octane gasoline. They postulated that methanol would be activated possibly to either the methyl cation (CH_3^+) or carbine ($:CH_2$). This highly active reactive intermediate would then add to the alkane. [21] Although they found the MTO products instead of the high-octane gasoline, several suggestions about the mechanism are variations on the one proposed originally by Chang and Silvestri (see Figure 7). There are several on carbenes [21]–[23] and carbocations. [24], [25]

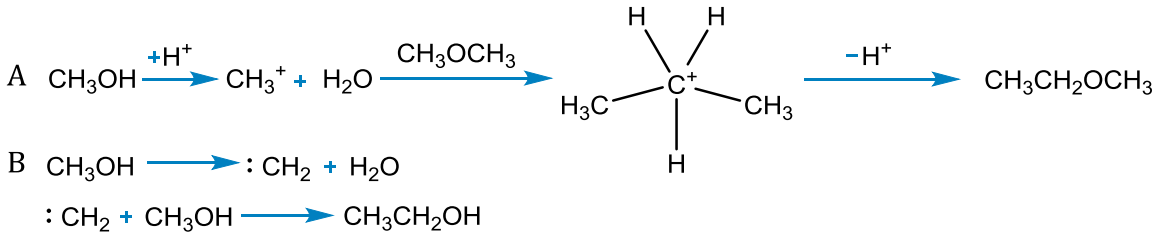

Figure 7. Classical 'direct' mechanism proposals. A) shows the pathway showing a carbenium ion alkylating DME to form a carbonium ion. B) shows one of several carbine pathways. Reproduced from ref [16]

There were also proposed mechanisms suggesting oxonium ylides [26]–[29] and free radicals (see Figure 8). [30], [31] However, these direct C-C bond formation mechanisms have little experimental evidence and theoretical methods show high-energy barriers, making the mechanisms unlikely. [32]–[36] Oxonium ylides are shown to form (at high loadings) from DME but NMR studies revealed it was reverted back to DME as temperature increased. [37] Also trimethylsulfonium and trimethylselenonium cations didn't accelerate the MTO process further tackling the proposal of oxonium ylides as active reaction intermediate. [38]

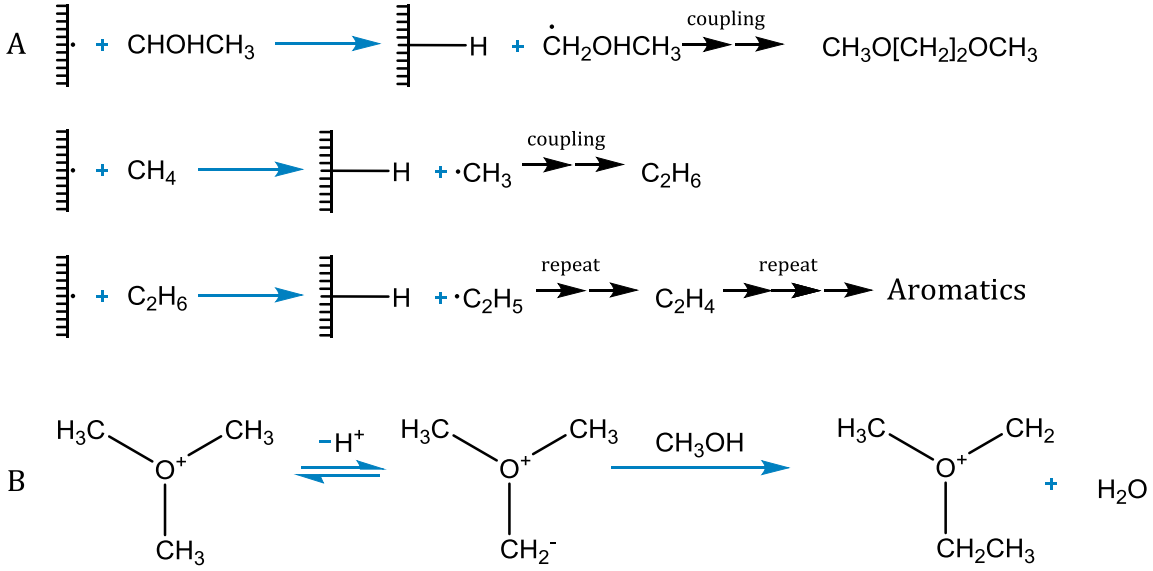

Figure 8. Schematic abbreviated proposals of: A) surface-radicals & B) oxonium ylide mechanisms, reproduced from ref [16] and ref [31]

It's been shown that methanol can react on the acid sites to form framework bound methoxy (methoxonium) species. [39]–[41] Although methoxonium groups might play an intermediate role in the first C-C bond formation, the actual alkoxy chain growth process (see Figure 9) has never been observed directly.

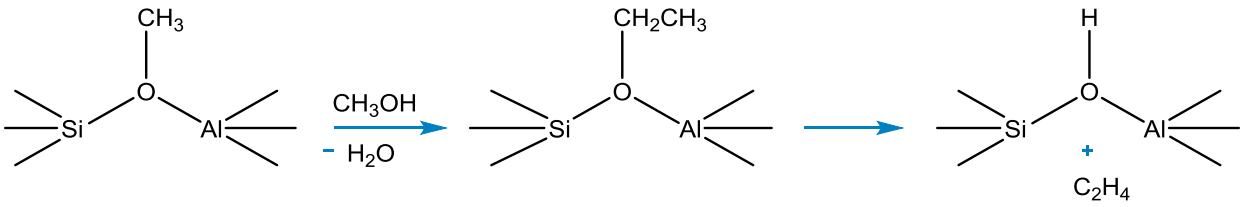

Figure 9. A proposed alkoxy chain growth process on a zeolitic active site, reproduced from ref [16]

During MTO reactions the initial rate of methanol conversion is decreased by orders of magnitude when using reagents, carrier gasses and catalysts purified from C-C bond containing species. Therefore it is likely that the direct formation of C-C bonds from methanol or DME is not important during steady-state conversion and, when using normal ('unpurified') feedstocks, during the induction period (period in which conversion is increasing) as well. Possible C-C bond formation using methanol or DME has probably no significant influence compared to the co-reaction of methanol with hydrocarbon impurities, which will be elaborated on later.

In a recent study, Comas-Vives et al. claim opposite and state to have found an answer on the uncertainties of the first carbon-carbon bond formation. [42] Using spectroscopy with a computational approach, γ-Al_2O_3 was studied when DME was fed. The Lewis-acidic sites on the 110-facet of γ-Al_2O_3 activated DME to yield CH_4, alkenes and surface formate species according to IR and NMR data. Oxonium ions are key reaction intermediates, and form upon reaction of methoxy surface species with coordinated methanol on adjacent alumina centers. This study suggests adjacent alumina cooperate and Al_2O_3 can participate in hydrogen transfer and C-C bond formation. Impurities would therefore be unnecessary to initiate the MTO-based reactions. However, since the Si/Al ratio plays such a vital role in affecting the MTO products (Zhu et al. [43] & Izadbakhsh et al. [44]) and lowers the amount of adjacent alumina, it can't be taken for granted that the formation of the HCP is solely due to DME activation in zeotype catalysts.

1.3.2 Hydrocarbon Pool

All described direct mechanisms lack an explanation concerning the observed induction period. Some believed a direct reaction was the foundation for more complicated auto-catalysis reactions through olefin chain growth and cracking. First, necessary alkenes are formed during the induction period. [45], [46] Then all ethylene and higher alkenes are formed by repeated methylations, oligomerizations and cracking. Cyclization reactions and hydrogen transfers would lead to aromatics and alkanes. [12] It was until 1982 that an alternative to this alkene-based model was proposed. Not alkenes, but toluene or p-xylene were added in small amounts leading to enhanced methanol conversion over a H-ZSM-5 catalyzed MTO-reaction. The proposed mechanism (see Figure 10) was called aromatic co-catalysis. [47], [48]

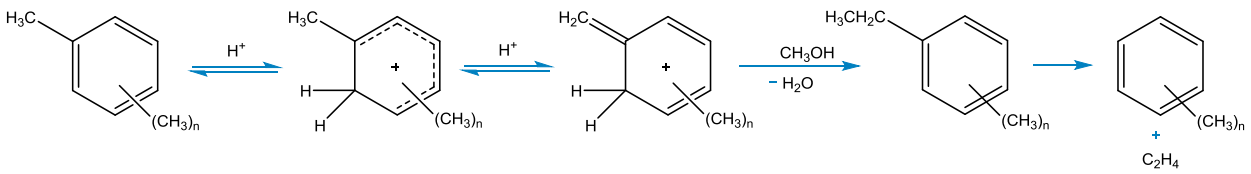

Figure 10. Schematic mechanism of aromatic co-catalysis, reproduced from refs [47], [48]

In the same period the influence of small amounts of higher alcohols on the duration of the induction period was studied. [49] The results were similar to the results of adding toluene and p-xylene: when 3.6 * 10^{-3} mol% of cyclohexanol was added as co-feed an 18-fold reduction of induction period was observed. Additionally, it was known that under MTO reaction conditions propylene is able to form cycloolefins. From this it was speculated that the first olefins formed in methanol conversion catalysis are from impurities in the feed. [49]

Using isotopic labeling, it was shown that ethylene and propylene had little reactivity when co-reacted with methanol over H-SAPO-34. [50]–[52] However, it was later shown that propylene had higher reactivity on H-ZSM-5. [53] This low reactivity led to the Hydrocarbon Pool mechanism (HCP) by Dahl and Kolboe. The HCP (see Figure 11) was said to may have many similarities to coke and contains less hydrogen than first indicated. The initial specified overall stoichiometry $(CH_2)_n$ was not further specified. [50]–[52]

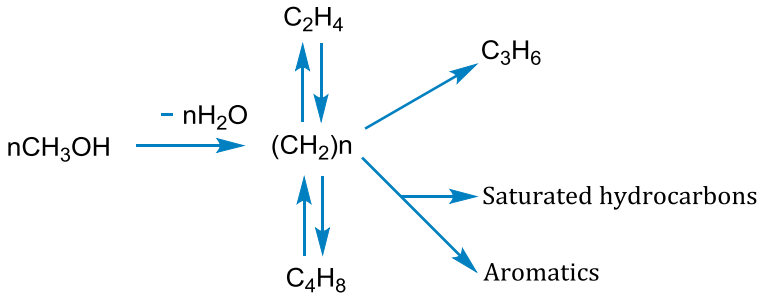

Figure 11. The hydrocarbon pool mechanism as originally proposed by Dahl & Kolboe

Parallel studies, by Haw & colleagues and Kolboe & colleagues, identified methylbenzenes as organic reaction centers for MTO reactions. [54]–[59] Arenes, or some arene derivatives, were found to play a significant part in the propylene formation. [60] When the reactivity of polymethylbenzenes over zeolite H-beta (12-membered ring, larger poresize than H-SAPO-34 and H-ZSM-5) was investigated, the heptamethylbenzenium (heptaMB$^+$) cation was found as key intermediate in the HCP. [61]–[64] As suggested by Langner it was also confirmed and shown that impurities play a major part as precursors in the HCP. [20], [65], [66]

More specific research on the broad HCP mechanism resulted in the following sections about the Paring & Side chain mechanisms. It must be noted that there is an alkene cycle (Figure 12), but this seems to have negligible influence on mechanisms for CHA-structured catalysts and

more relevance for ZSM-5. [1] Therefore there won't be any further elaboration on this alkene-cycle.

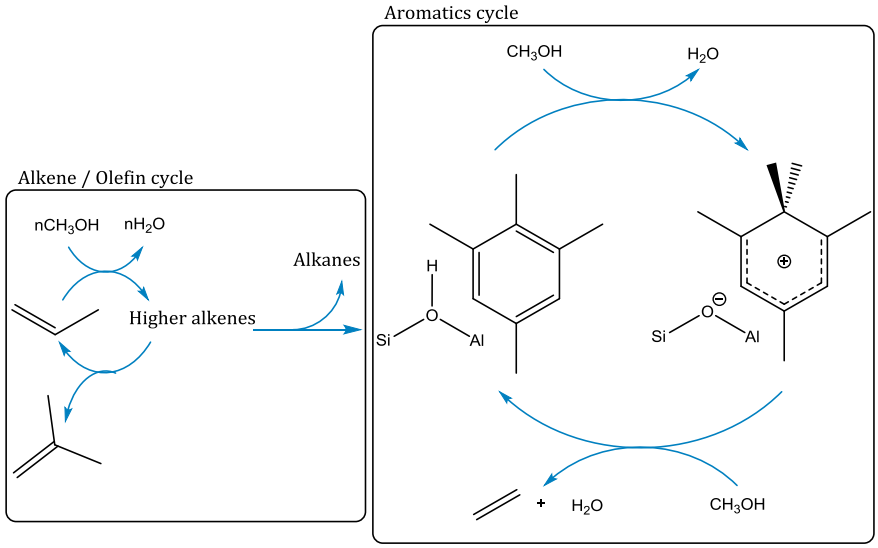

Figure 12. HCP mechanism showing both alkene and aromatics cycles. The aromatics cycle can be understood as 'paring' or 'side-chain' mechanism as will be elaborated on in the following sections. Reproduced from ref [42].

1.3.3 Paring Mechanism

To elaborate on the product distribution in the hydrocracking of aromatic hydrocarbons, Sullivan & colleagues proposed the paring mechanism (see Figure 13). [67] This mechanism can be displayed as a catalytic cycle: first ring contraction followed by expansion. This creates the opportunity to extend an alkyl chain and thus eliminate an olefin. The mechanism can be imagined by thinking of a methylbenzene where methylgroups are 'shaved off' as alkenes. The mechanism gain direct evidence by studies using mass spectrometry. [68], [69] This reaction is playing only a minor role in olefin production, although recent research has shown that all methylbenzenes can eliminate olefins via this mechanism, where having less methyl-substituents account for a higher energy barrier. [16], [70]

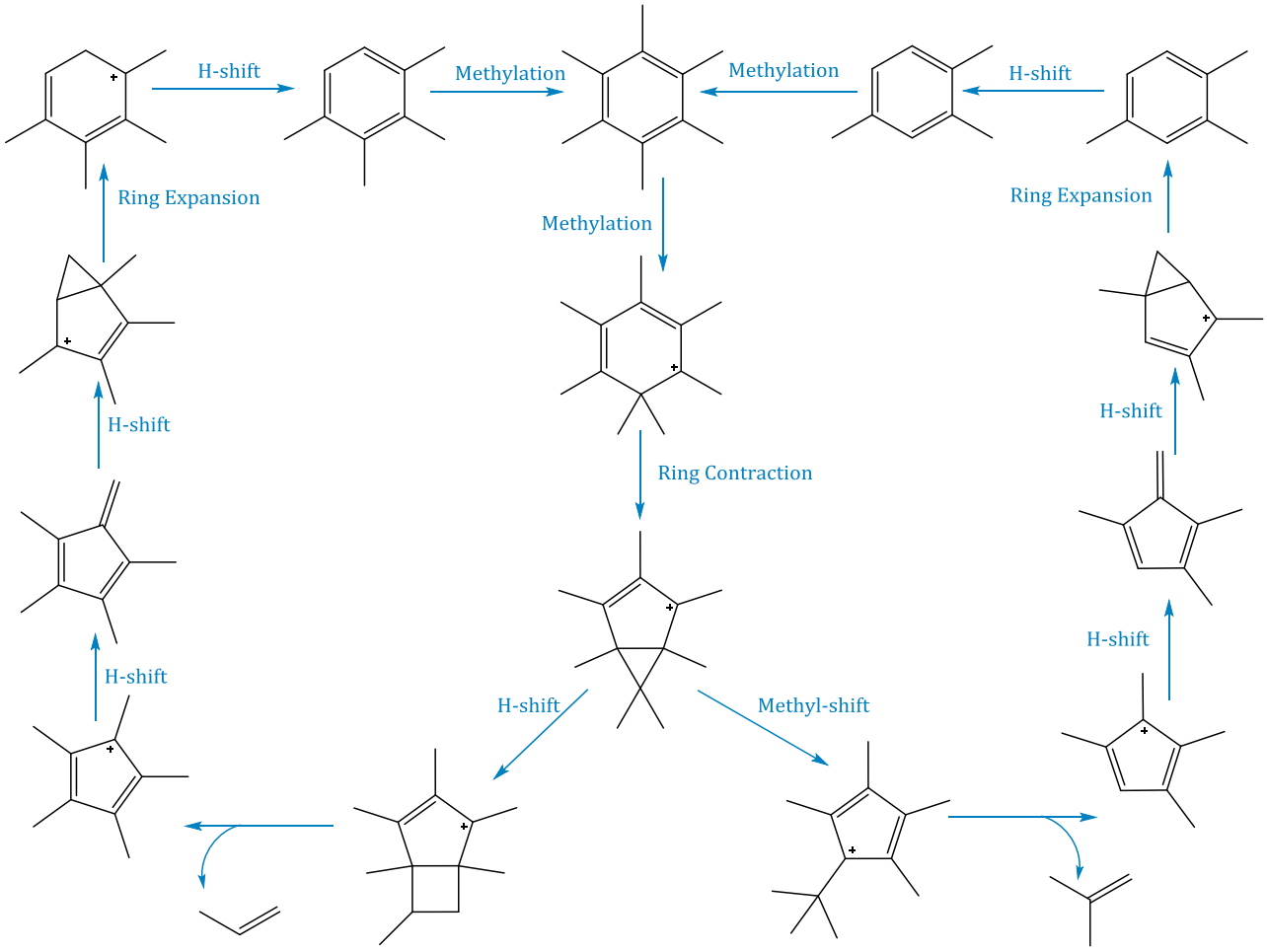

Figure 13. Paring mechanism from hexamethylbenzene (HMB), producing isobutene and propylene, reproduced from ref [70]

1.3.4 Side Chain Mechanism

In parallel of the paring mechanism as described above, the side chain mechanism is another pathway in MTO reactions. Both Mole & colleagues and Haw & colleagues played an essential part in the formulation of this mechanism, which is nowadays believed to be the main source of olefin formation. [47], [48], [71]–[75] The mechanism as in Figure 14 is based on the HMB co-catalytic species (colored in turquoise).

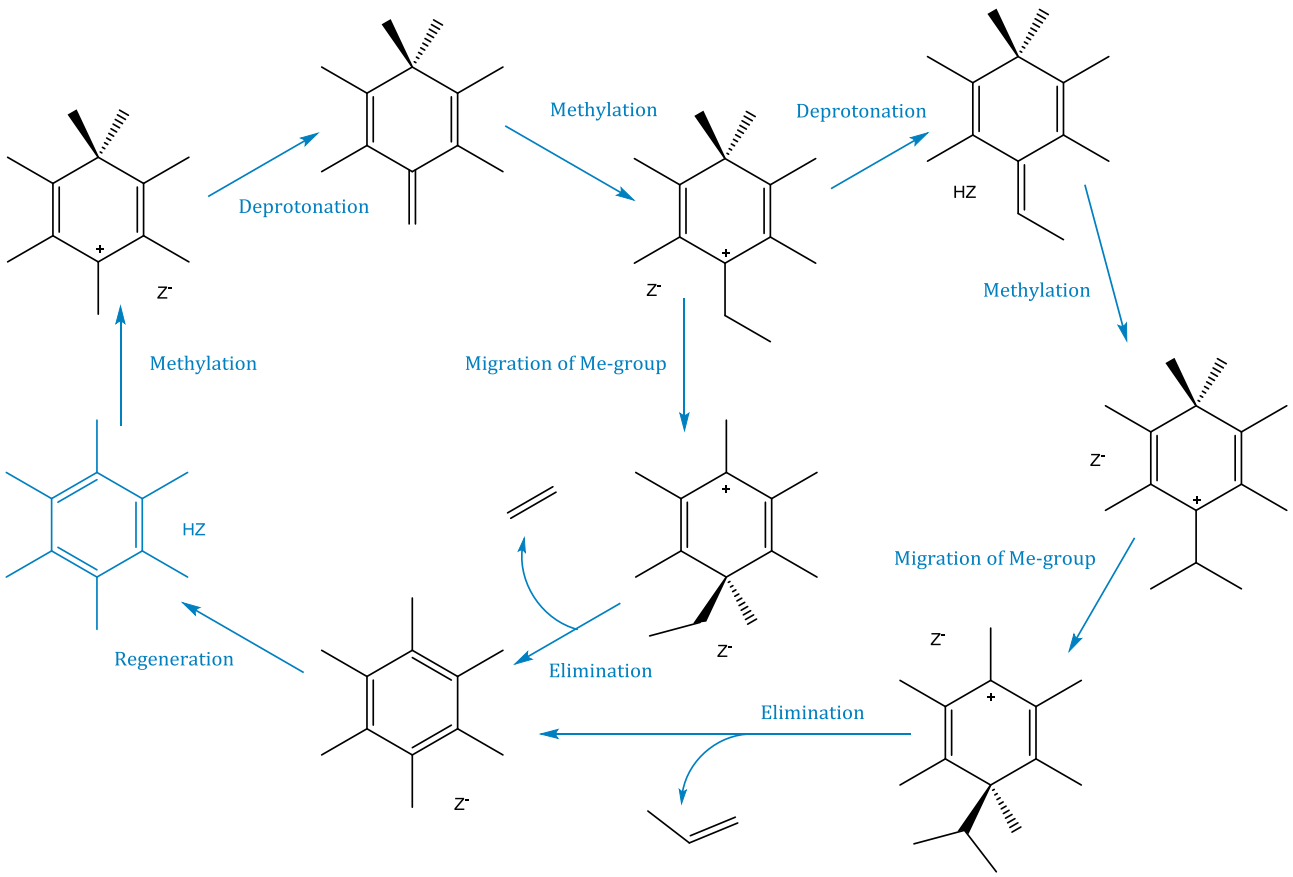

Figure 14. Side chain mechanism for HMB, producing light olefins, reproduced from ref [72]

First, the HMB is methylated to form a (heptaMB$^+$) cation. This process is either initiated by the formation of methoxy species adsorbed on the acid sites, (protonated) methanol molecules or DME. The heptaMB$^+$ cation gets deprotonated in its para position to form 1,2,3,3,4,5-hexamethyl-6-methylene-1,4-cyclohexadiene (HMMC). In a next step, the HMMC is methylated on the exocyclic double bond to form an ethyl side-chain. The gem-methyl group (in para position with the exocyclic double bond) migrates towards the ring carbon where this ethyl side-chain is connected. A sp^3-hybridized ring carbon atom is formed and the C-C bond, which needs to be broken to split off ethylene, is weakened. The ethylene is eliminated and the terminal methyl group of the ethyl side chain is deprotonated. This step is assisted by water molecules. [72] The formation of propylene is similar, apart from the fact that the product of the first methylation undergoes an additional deprotonation and methylation, giving rise to the propyl side chain. It should be noted that the products of the elimination steps still contain a H_3O^+ cation explaining the Z^- presence at the end of the cycles. [72] Propylene is expected to be the main product when doing energy-calculations and this is in line with the majority of MTO research. [5], [71]–[73], [76]

1.3.5 Coke formation

The main contra argument for using zeolites or zeotypes as catalyst for MTO reactions is deactivation. Zeolites or zeotypes are known to deactivate quickly, because their shape selective framework leads to problems like pore blockage and the filling of cavities, blocking the internal active sites (Figure 15A). Species in the HCP are shown to be precursors for coke formation. Several studies have shown that reaction conditions affect the activating or deactivating nature of a type of species (Figure 15B). [11], [77] When these precursors undergo addition reactions and grow to larger species that show no activity in olefin production, they're defined as coke. A few of these species are highly (>5) methylated naphthalenic, phenantrenic or pyrenic species. [18]

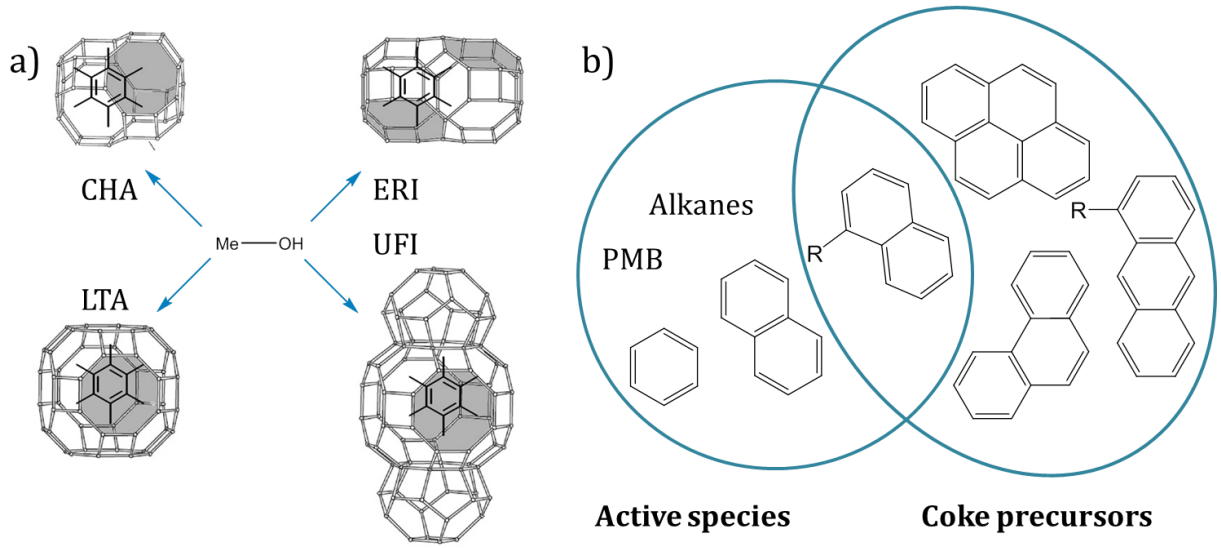

Figure 15. A) Different 8-membered ring molecular sieves cages with HMB compared. Reproduced from ref [78] B) Role of HCP species in zeolitic cages during the MTO reaction. Reproduced from ref [79]

1.4 The influence of water

Many catalytic processes using zeolites are influenced by water. Cracking, cyclization, oligomerization, alkylation and isomerization are all phases occurring in the (formation of the) HCP. Although recent studies focus on the influence of water on reactions catalyzed by solid acid materials, like zeolites, most are using water as diluent or reagent in liquid phase. [80]–[84] Consequently, the results are unreliable when stating they should be of influence on the MTO reactions as well. Remarkable is the small amount of studies on the effect of water on MTH processes, since water is stoichiometrically formed in the process. As justly stated by Chen et al., it seems inappropriate that "in essentially all mechanistic proposals, water has simply been ignored as a molecular participant." [85] Below will be a chronological summary of research done on MTO reactions taking water into account.

1.4.1 Water in feed or as diluent

Using ^{13}C MAS NMR, Xu et al. (1990) studied the product distribution under different conditions over a H-SAPO-34 catalyst. [86] They found the noteworthy effect that the ratio of olefins to paraffins differs with the rate of methanol feed and the M/W ratio. This rate is maximum for a certain range within weight hourly space velocity (WHSV) from $2h^{-1}$ up to $10h^{-1}$ and M/W ratios 30/70 & 40/60. The water also caused higher olefin yields (see Figure 16). This is stated to be a result of competition for the Brønsted acid sites between the different basic species. The basicity of water is significantly larger than that of methanol and olefins and therefore water is more likely to occupy stronger acid sites, leaving fewer and weaker acid sites in the catalyst. Xu et al. state that "the optimum ratio of water is a function of the hydrothermal stability of the structure and the conversion rate of olefins". [86]

Figure 16. Product distribution at 400°C with 40/60 and 100/0 M/W ratios, respectively (detected by GC). Reproduced from ref [86]

Me/Wa	**Products**						
	C_2H_4 (%)	C_2H_6 (%)	C_3H_6 (%)	C_3H_8 (%)	C_4H_8 (%)	C_4H_{10} (%)	$>C_5$ (%)
40/60	33.1	*	29.1	*	13.2	*	*
100/0	20.4	8.8	19.5	14.5	6.5	7.2	*

Around a year later, Dehertog & Froment (1991) did similar research on H-ZSM-5, studying the influence of different catalyst parameters and reaction conditions. [87] They varied the partial pressure of methanol by using diluents and came to the general conclusion that it gives rise to similar effects as influencing the temperature. The yield of light alkenes increases significantly when the partial pressure is decreased. This gain of yield is almost exclusively to the formation of propene, whose yield almost doubles. However, when using water as diluent instead of nitrogen, the ethylene selectivity increases slightly (3,4% to 6,6%), although the maximum yield of light alkenes was the same for both diluents. [87]

Van Niekerk et al. (1996) used water as diluent to test their synthesized SAPO-34 catalysts. When using water instead of high-purity nitrogen, they noticed a three-fold increase in catalyst lifetime, a reduction of methane selectivity and C_2/C_3 ratio (so more propylene) and essentially no change in olefin selectivity. [88] This seems to be contradictory to earlier (and later) results as described in this section.

Wu & Anthony studied the effect of feed composition on SAPO-34. [89] They hypothesized that water should increase ethylene selectivity, since this is primarily formed of methanol, while propylene is formed of DME and the methoxy-ion. [76] Since water shifts the equilibrium towards methanol, more ethylene should be formed. Their research resulted in decreased formation of coke and prolonged catalyst activity. The amount of processed methanol over catalyst increased from 0.21 g-methanol/g-catalyst (M/W = 1/0) to 1.67 g-methanol/g-catalyst (M/W ≈ 1/4) (see Figure 17). This means more than an eight times increase. Wu & Anthony explain this by polar water molecules occupying (strong) acid sites, making these sites unavailable to olefins which therefore can't undergo oligomerization and coking. [89] This explanation is similar to the one given by Xu et al. in 1990.

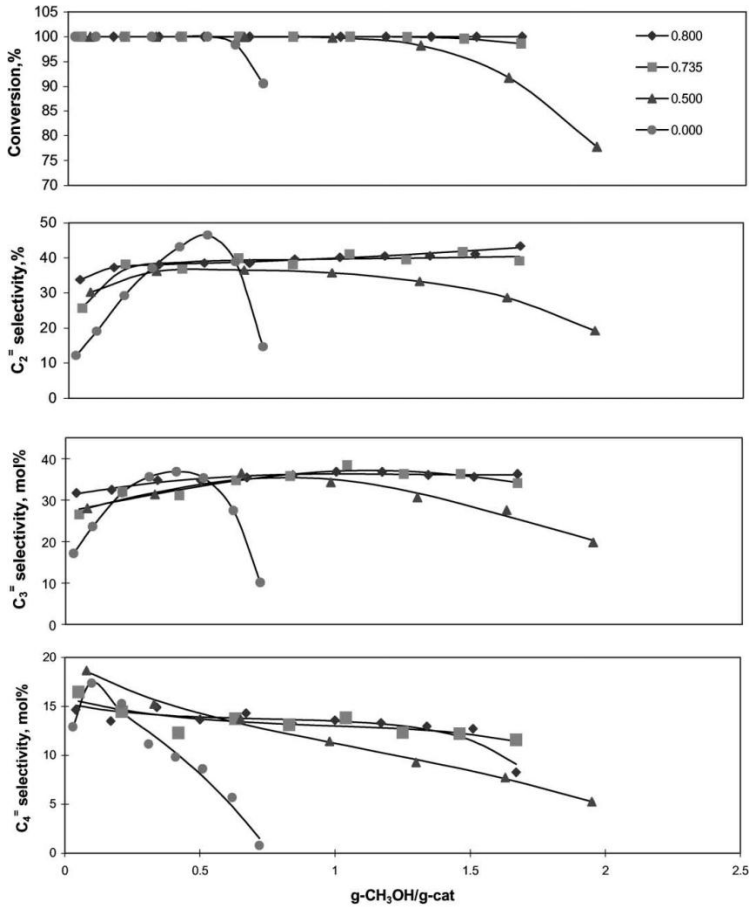

Figure 17. Influence of water in the feed on product selectivity and conversion. The values in the legend stand for molar factions of water in the Me/Wa feed. Reaction conditions; 400°C, LHSV = 6.75 hr^{-1} for Me/Wa feeds, and 1.5 hr^{-1} for pure methanol feed. From ref [89]

Wu et al. broadened this research by varying the different reaction conditions, also when using a M/W = 1/4 feed. [2] They concluded that optimal conversion takes place at approximately 400°C, using weight hourly space velocities of 2.6 – 3.6 h^{-1} over the SAPO-34 catalyst. In 2008, Shahda et al. confirmed the positive influence of water on the MTO reaction over SAPO-34. [90] They noted that a decrease in methanol concentration led to an increase in olefin selectivity. When adding water to the feed, the methanol concentration was subsequently decreased. They explained their increase in selectivity and decrease of deactivation by citing Dehertog & Froment (ref [3]). A study by Taheri Najafabadi et al. on the kinetics of MTO chain reactions confirmed the higher selectivity for ethylene. They stressed the flexibility of the process when adding different M/W ratios and noted that the only practical issue is the reduction of the net feed rate to the system by water in the feed. However, this can be solved by increasing the feed velocity. [91]

In an earlier work by this group, Wondergem studied the effect of water on MTO reactions. Her focus was mainly to study the effect of water on the induction period, HCP species and coke formation. Using in-situ microspectroscopy combining UV-Vis with microscopic imaging tests, H-SAPO-34 crystals (50 *50 * 50 μm^3) were monitored while feeding methanol with different ratios of water (1/0, 1/1, 1/2, 1/4, 1/8 and 1/12). In line with earlier results, the induction period increased with higher water ratios, interestingly with linear behavior. Looking at the microscopic imaging, it became clear that an increased and more homogeneous distribution of MTO intermediates was observed. Both increased induction period and distribution of intermediates can be explained by the competitive adsorption between methanol and water, but also propylene and water. [3] Since water adsorbs on the acid sites, the methanol (or formed olefins) are forced deeper into the zeotypes crystals, hence increasing the distribution (Figure 18).

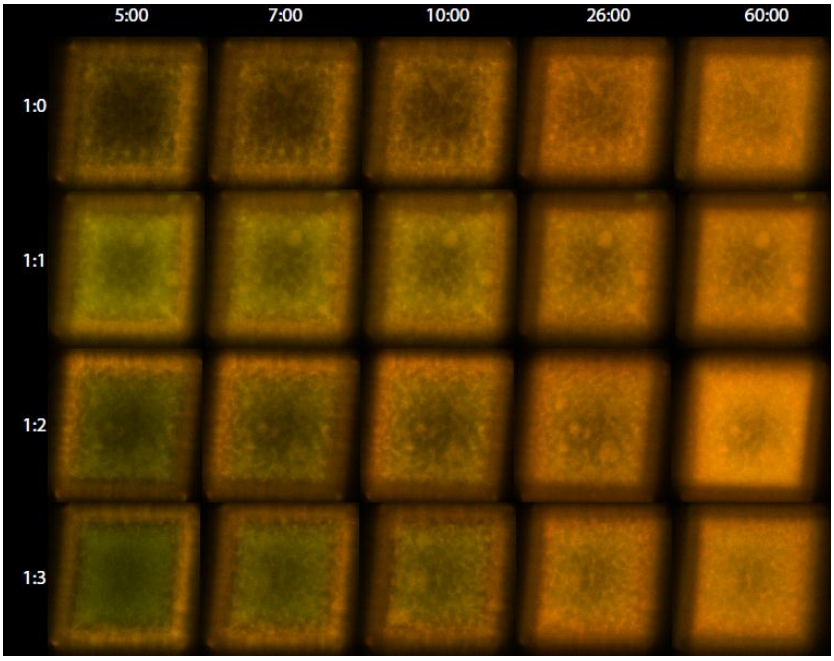

Figure 18. Increasing water content compared to TOS shows a more homogeneous distribution of fluorescent species for higher water loadings

As can be seen in Figure 18 a layer of fluorescent species seems to be present in the crystals, most noticeable for lower TOS. These layers can be viewed as a 'coke crust'; an outer layer of deactivated species blocking the pores and therefore catalytic performance of the crystal. As in line with earlier explanation of competitive adsorption, one would expect the coke crust to be thicker for higher water loadings since methanol is diffused deeper into the crystal. Measuring the coke crusts (Figure 19) in the images of Figure 18 indeed showed an increased thickness of coke crust.

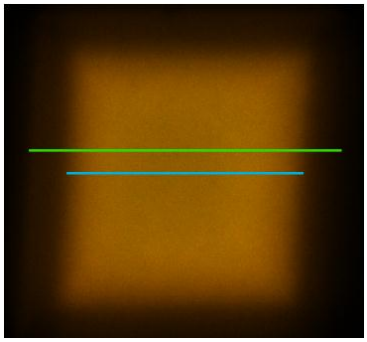

Figure 19. A single SAPO-34 crystal. The total width is indicated by the green line. The blue line shows the part without coke crust

Furthermore UV-Vis results showed more occupied Brønsted acid sites, a change in ratios of HCP species and a decrease in the shift of the framework vibrations strengthening the assumption of competitive adsorption.

1.4.2 C-H bond activation

The acidic zeolite H-ZSM-5 is able to activate alkane C-H bonds at ambient conditions. [92], [93] The effect of water on this bond activation was studied by Chen et al. [94] Although they emphasized that earlier studies have suggested that water effectively acts as a poison, they show that water not only suppresses but also may enhance alkane reactivity in zeolites. [95] With the use of ^{1}H MAS NMR Chen et al. showed that the presence of ca. 1 water molecule per acid site increased the rate of isobutane bond-activation with an order of magnitude. Furthermore, increasing the water content to more than 1-3 equivalents reduced the alkane reactivity. Even higher water loadings suppressed the reactivity completely.

The suppression of reactivity can be explained by the clustering of water molecules at the acid sites. The proton affinity for water dimers and trimers is much higher (200-230 kcal/mol) than for isobutane or a single water molecule. [94], [96] The formed clusters will therefore prevent access for isobutane at the acid sites. Conclusively, one would expect beneficial effects of water in zeolite-catalyzed hydrocarbon reactions at low loadings. The results from this study indicate that water can play an important role in reactions involving hydrophobic molecules in solid acid catalysts, possibly via transition state stabilization. These conditions are also present in MTO reactions.

1.5 Thesis Aim

The aim of this thesis is to eludicate on the role of water in the MTO reaction. Water might influence all scales of the process; diffusion, physical interaction on acid sites and the chemical interaction with reagents, intermediates or products. Based on operando UV-Vis to marry the catalytic performance to hydrocarbon formation in the catalyst particles, an in-depth analysis will be done on several methanol / water ratios to inspect the nature of water in the process. The aim is therefore not only to focus on the catalytic improvement (if any) obtained from water on the feed: it is focused on explaining why water has such a pivotal influence and how this interaction can be explained. A beginning for such assumptions to be made is found studying the effect of methanol concentration, with a stable space velocity, clarifying the difference between physical process influence (more diluent) with chemical, or molecular, process influence (water added in the diluent).

Chapter 2 – Experimental

2.1 Catalyst preparation

Before catalytic testing on MTO reactions was performed, the catalysts were calcined. H-SAPO-34 of ACS Materials (see Table 1 for properties) was used. The SAPO-34 was calcined in an air-flown tube oven heating to 393 K with a ramp of 1 K/min (Figure 20). There it was kept constant for 2 h. Thereafter it was heated to 853 K with a ramp of 3 K/min. This calcination temperature was kept constant for 6h, before cooling down to room temperature.

Table 1. Properties of used H-SAPO-34 from ACS Materials

Properties	**SAPO-34**
Pore Volume (cm^3/g)	≥0.27
Average Particle Size (μm)	2-15
T ratios	2.25 (Al+P/Si)
Cation	H

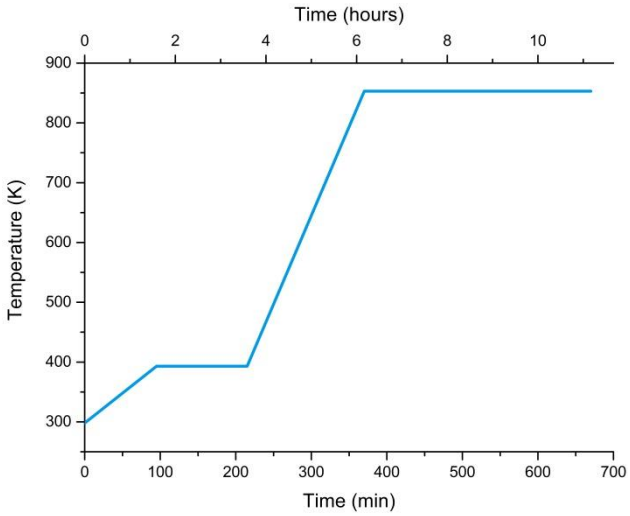

Figure 20. Calcination procedure for SAPO-34

After calcination, the zeotype catalyst was pressed to give pellets, followed by crushing and sieving. Only particles with sizes ranging from 212 – 425 μm were used in the reactions. Smaller particles may initiate a pressure drop in the reactor and might be forced through the reactor holder, blocking the gas lines. Larger particles may give diffusion limitations, lowering the activity of the catalyst particles.

2.2 Catalyst characterization

To obtain a clear set of characteristics catalyst, different characterization methods were applied before performance tests were done.

2.2.1 NH_3-TPD

The acidity of the different zeotypes was measured using temperature-programmed desorption (TPD) using ammonia as probe molecule. This was measured using a Micrometics Autochem 2910 apparatus. 100 mg of the calcined and sieved catalyst was placed in a quartz tube reactor and preheated at 823 K under 25 mL/min of He flow for 30 minutes. Ammonia (10 vol % in He) was adsorbed for 45 minutes at 373 K using pulses. The physisorbed ammonia was flushed with a He flow of 50 mL/min for 2 h. Afterwards desorption was measured using a thermal conductivity detector (TCD) while the sample was heated from 373 – 873 K at a heating rate of 5 K/min under He flow.

2.2.2 CO Adsorption FTIR

Fourier transform infrared (FTIR) measurements have been done while probing the different catalysts under CO pressure to describe the local structure of acid sites in the CHA type materials. The absorption of CO as base (via the carbon end) shifts the bands related to Brønsted acid sites to lower frequencies with a shift proportional to their acidic strength. [97] In a similar fashion, the C-O stretching frequency is shifted to higher values, although this research focuses only on the peaks representing framework O-H groups (so not the probe molecule). Self-supporting wafers were made using 10-15 mg of catalyst. The wafers were first activated by heating to 673 K with a ramp of 5 K/min under vacuum ($\sim 10^{-5}$ mbar) while spectra were periodically recorded to monitor the amount of water in the wafer. After an hour at 673 K, the wafers were slowly cooled to room temperature and further cooled down by circulating liquid nitrogen around the cell. When the temperature was stabilized around 90 K, CO (10% in He) was added and stabilized at increasing pressures. Spectra were recorded at different pressures.

2.2.3 XRD Powder diffraction

The SAPO-34 was analyzed using a Bruker D8 X-ray powder diffractometer with variable slit. This diffractometer was equipped with a Co Kα X-ray tube (λ = 1.79026 Å)Co X-ray tube. XRD patterns were recorded in the range of 5 – 45 ° 2Θ at room temperature with steps of 0.02°. Diffractograms were only used to give qualitative information about the framework type present in both catalysts.

2.3 *Operando UV-Vis measurements & analysis*

The MTO reactions have been performed in a fixed-bed quartz reactor (see Figure 21 and Figure 22). 50 mg of prepared catalyst (as described above) was used for the reaction and placed in the reactor. Before performing the reaction, the catalyst was activated at 823 K under 100% oxygen flow (10.00 mL/min) for 1h and then cooled to reaction temperature while flushing away the oxygen using helium (40.00 mL/min). The methanol was added using helium as carrier gas, flowing it through a saturator of methanol which was kept approximately around 303 K. The water was added through a parallel flow, using helium as carrier gas through a water saturator kept around 339K. Following the ideal gas law and Antoine's equation, this makes the concentration for both water and methanol vapors approximately 0.008 mol/L in the saturators (see Appendix A, page 64, for a complete calculation). The gasses are flown in different ratios and completed to a total flow of 110.00 mL/min with an external nitrogen-line, making the WHSV ≃ 4 g/(g.h). These three lines combine and are 'stabilized' before starting the reaction; the reagents flow was put through a reactor-bypass to the GC, until the level of oxygen (and methanol) was stable. The temperature of the reactor was 673 K. GC analysis was done by using an Interscience Compact GC instrument equipped with Rtx-1+Rtx-Wax columns and Rtx-TCEP+Rtx-1 and Al_2O_3/Na_2SO_4 columns, respectively, and two flame ionization detectors (FIDs).

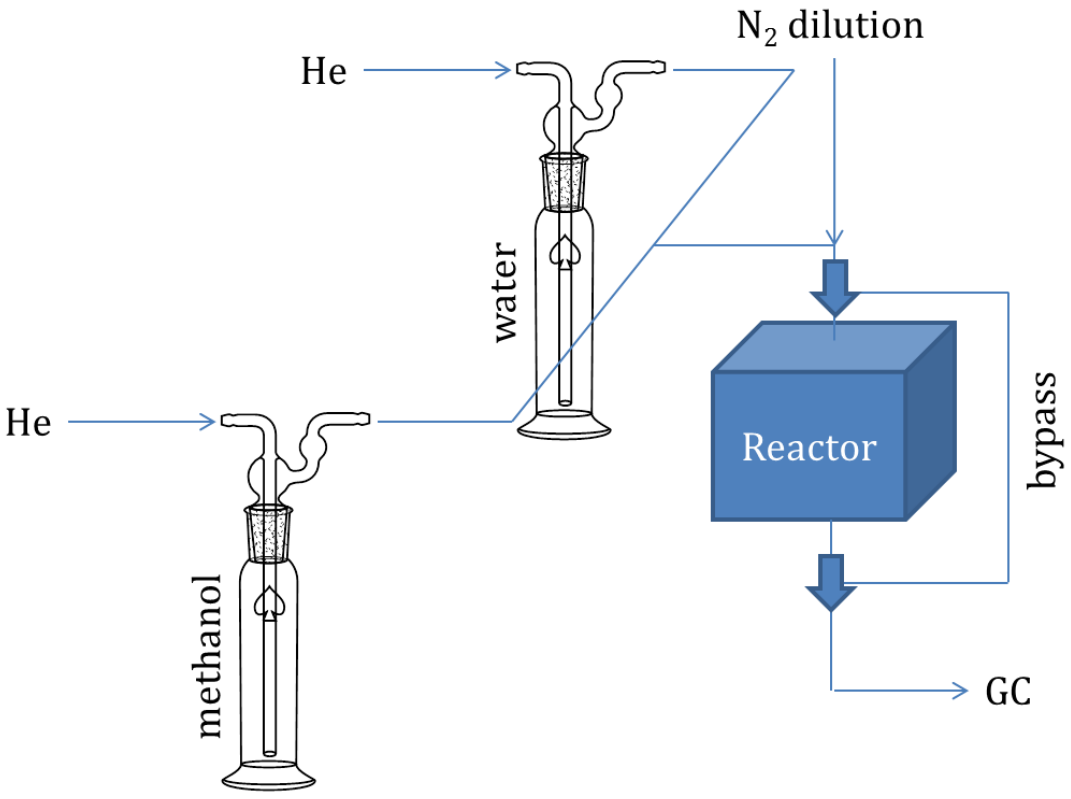

Figure 21. Flow scheme of the MTO in-situ setup. The thick arrow indicates a three-way valve. Helium and nitrogen flows were controlled using a mass-flow controller.

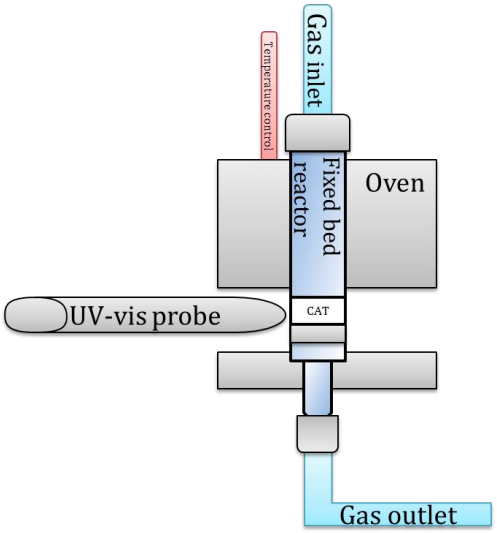

Figure 22. 'Reactor' part from **Figure 21**

UV-Vis measurements were performed in the wavenumber range of 12500 – 38600 cm^{-1} / 260 – 800 nm using an UV-Vis probe provided by Avantes. The probe consists of one excitation and one collection optical fiber with a size diameter of 400 µm and a length of 1.5 m. The probe was connected to a deuterium-halogen light source and an AvaSpec 2048 UV-vis spectrometer. AvaSoft 7.7 was used as supportive software and spectra were saved every 30s (≃ 5 UV-Vis recordings per GC measurement) with an integration time of 400 ms and averaged based on 75 recordings. Three different periods were defined, as explained in Figure 23.

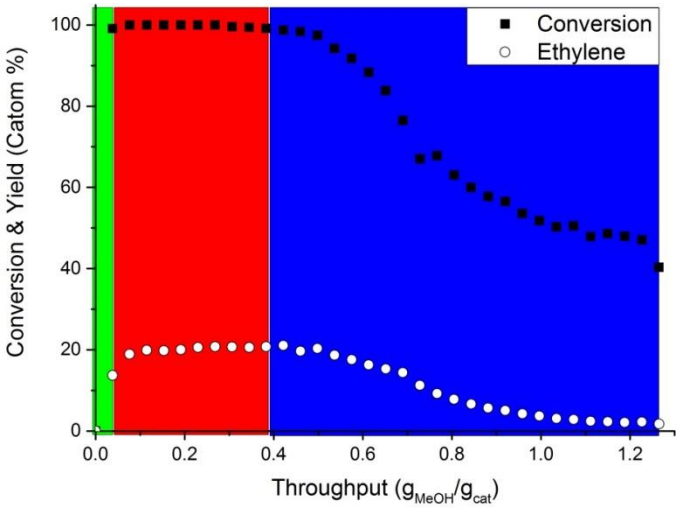

Figure 23. Three different periods are defined during experiments. The induction period (IP) in green are data points measured when methanol conversion rises from 0% to 1.5% under the maximum conversion. The active period (AP) in red is defined as the period wherein conversion is within the conversion(max) to conversion(max-1.5%) range. The deactivation period (DP) in blue starts when conversion drops 1.5% below the conversion(max). The catalyst is defined as deactivated when C_2% is 1/10th of its maximum.

Non-negative matrix factorization, or NNMF, analysis was done on the UV-Vis spectra recorded. NNMF is a powerful analysis method ([98], [99]) to factorize a data matrix T x W into two matrices X (T x k) and Y (k x W) with the condition that all matrices have only positive elements, as explained in ref [77]. In this work the data matrix consists of wavenumber (W) x time (T). Using the NNMF analysis gives us the numerically approximated result X*Y, which is a lower rank approximation of the data matrix.The rows of k*W are called 'eigenspectra', identifying groups of bands which share a similar advancement in time. This advancement in time can be thought of as 'kinetic profiles', and these are formed by minimizing the root-mean-squared residual between the data matrix and X*Y using an alternative least squares (ALS) algorithm. For these NNMF plots, an ALS of 100,000 was used and two and three rank approximations (k=2 & k=3) were analyzed.

Propylene feeding experiments were in a similar fashion as the operando MTO measurements. These experiments have the same experimental setup, conditions vary however. Propylene (purity 2.5 / 99.5%) gas was flowed over the catalyst. Due to experimental limitations, the minimum flow of propylene was 2.34 mL/min. The propylene stream was diluted with the external dilution (or water) line to a total flow of 110 mL/min. This made the average propylene concentration in the flow 2.3% (determined by GC) with a space velocity of approximately 5.2 g/(g.h), which is similar to the methanol WHSV (see Appendix A, page 64, for the calculations). Two experiments were performed; the first consisted of propylene with water (1/1 ratio) in order to mimic the product stream of a MTO reaction. Water was added through 100 mL/min flowing through a saturator with T = 298 K. The second experiment was propylene with an increased amount of water using this saturator at T = 338 K (1/9 ratio, which is 3 times the stoichiometric amount). UV-vis for these propylene-feeding-experiments were recorded every 7 seconds, with an integration time of 70 ms and averaged based on 100 recordings. The runs were all allowed to run for 1.5 hours; since time couldn't be normalized on methanol throughput, the time was fixed.

2.4 Thermogravimetric Analysis

To analyze the amount of coke in the deactivated catalyst after reaction, thermogravimetric analysis was used. After the MTO reaction 10 – 15 mg of deactivated catalyst was used for TGA. The sample was heated to 50°C under 20.00 mL/min N_2-flow and kept for 10 minutes under these conditions. The sample was then heated to 750°C with a ramp of 5°C/min and under 10.00 mL/min O_2-flow. The sample was kept at these conditions for another minute. The analysis was done using PerkinElmer Pyris 1 TGA combined with an MS detector. With MS, the concentration of CO, CO_2 & H_2O was monitored during the analysis.

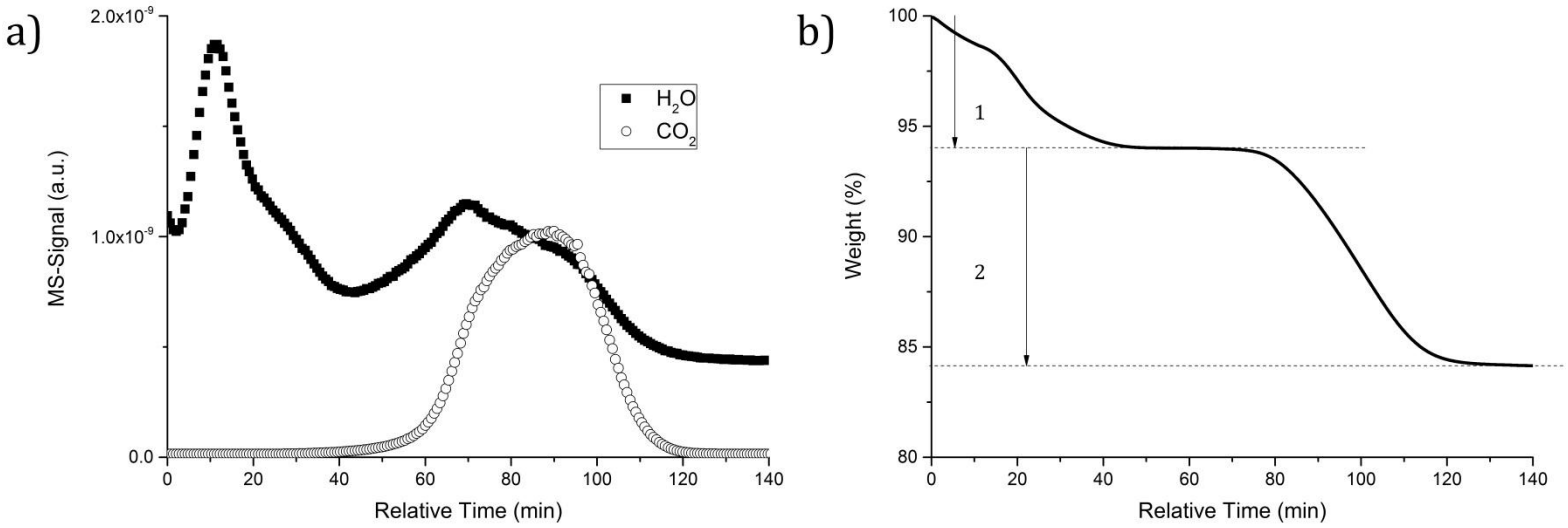

Figure 24. a) MS plot, recording species detected during TGA, plotting the intensity of MS signal versus the relative time. b) TGA of a deactivated SAPO-34 sample after MTO reaction, plotting the weight percentage versus the relative time

During the first 40 minutes, we see a large weight loss for water in Figure 24 which is indicated by the arrow 1. The loss of weight is due to adsorbed water instead of a reaction step. The second weight loss, indicated by arrow 2, can be explained by the burning of hydrocarbons. This is confirmed by the increase of the CO_2 MS signal. Taking the lower (dashed) line of arrow 2 as lower weight limit, and upper (dashed) line as higher weight limit, the grams of coke per gram of catalyst can be calculated with the following formula, assuming all coke is burned off during the TGA:

$$\frac{(Higher\ weight\ limit - Lower\ weight\ limit)}{Higher\ weight\ limit} = g_{coke} \cdot g_{cat}^{-1}$$

Chapter 3 – Results & Discussion

3.1 Catalyst characterization

The properties of the H-SAPO-34 catalyst is elaborated on in the following section. Results of different characterization methods are discussed and explained.

3.1.1 NH_3-TPD

In order to determine the acidity of the materials, NH_3-TPD was done on the acidic H-SAPO-34 catalyst. The plotted figure below shows the TCD concentration (a.u.) versus temperature (K).

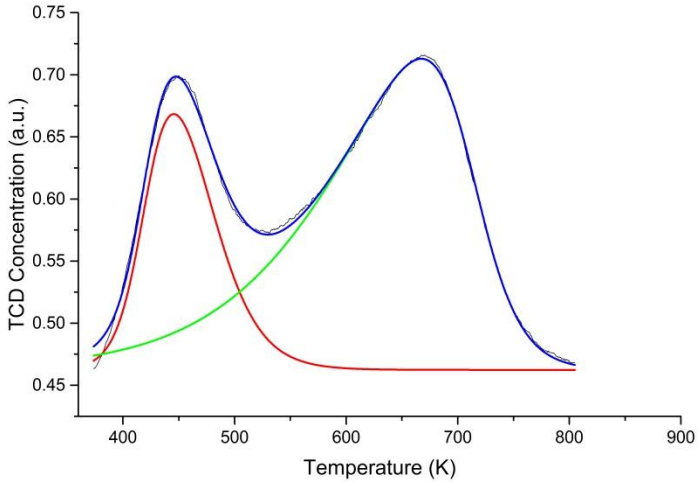

Figure 25. NH_3-TPD plots of SAPO-34. The blue line represents the sum of deconvolution (anti-sym. function) fits while the red and green lines are the deconvoluted peaks. The y-axis represents the amount of NH_3 concentration detected, while the x-axis shows the course of temperature

The catalyst shows two intense NH_3 desorption bands. These bands represent a certain nature of acid sites, where a higher desorption temperature means a stronger acid site.[77], [100], [101] Although all physisorbed ammonia should be flushed away, previous papers report that the peak around 450 K can either be assigned to physisorbed ammonia [102], or adsorbed ammonia on weaker (Lewis) acid sites.[100], [103] The peak at higher temperatures (670 K) should correspond to the stronger Brønsted acid sites.[100], [101], [103] Assuming one molecule of ammonia is desorbed from one strong acid site, the amount of desorbed ammonia gives a direct measure of strong (Brønsted) acid sites in the catalyst material. Since there might be an overlap between the different peaks, a deconvolution was performed. The deconvolution was done in Origin, using "Multiple Peak Fit" > "Asym2sig" to get an optimal fit (adj. R^2 = 0.998). The total amount of area (blue plot) is 59.488 a.u. corresponding to 30.02 cm^3/g (STP). The deconvoluted stronger acid sites peak (green plot) has an area of 40.691 a.u. and therefore the total amount of desorbed ammonia corresponding to the stronger acid sites of SAPO-34 is 20.53 cm^3/g (STP). Following earlier assumptions, the position of the peaks gives us more detail about the nature of the acid sites. H-SAPO-34 has an overlap of peaks corresponding to "strong" and "weak" acid sites and therefore seems to desorb at a wide range has a weaker, less well-defined acid strength. However, the amount

of Brønsted acid sites is theoretically calculated 0.917 mol NH_4^+ per gram of catalyst (see Appendix A, page 64). This value suggests 55% of the silica atoms in the catalyst are responsible for Brønsted acid sites.

3.1.2 CO Adsorption FTIR

Figure 26 shows only two different CO-pressures on the different catalysts (see Appendix B, page 66, for all increasing CO doses and the whole 4000 – 1500 cm^{-1} range). The shown spectra are both in the stage where strong Brønsted sites interact with the CO, instead of the interactions with silanols and/or polyadditions.

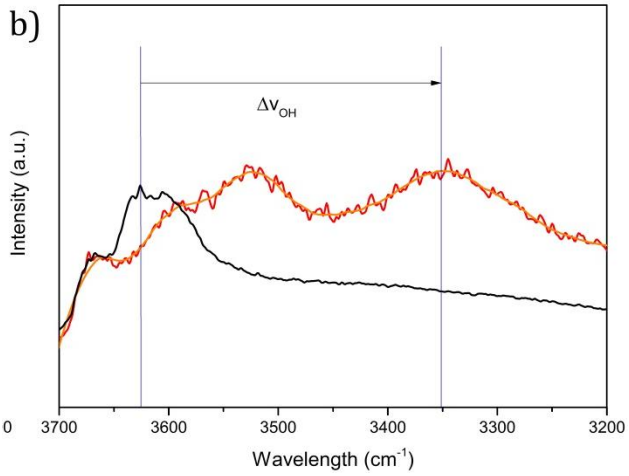

Figure 26. FTIR spectra of SAPO-34. Black represents low CO-pressure (0.014 mbar) while red represents higher CO-pressure (0.25 mbar)

Looking at the FTIR spectra(Figure 26A) at low CO pressure we can identify several peaks. There's the high-frequency (HF) component of Brønsted acid sites around 3615 cm^{-1}, representing ν_{OH} modes virtually isolated silanol groups located on the internal or external surface of the zeolite. The low frequency (LF) component of Brønsted acid sites at 3590 cm^{-1} represents silanol groups where only oxygen participates in H-bonding. Finally, there are H-bonded silanols (also described as silanol nests) represented by the broad peak around 3500 cm^{-1}. [97] When the CO pressure is higher, we can see that the left part of the original HF/LF components seems to be consumed. Besides, the right side seems to be consumed as well, but at a weaker magnitude. We can see the rise of two bands around 3523 cm^{-1} and 3351 cm^{-1}. The band at 3351 cm^{-1} represents red shifted modes of OH---CO adducts. Taking the HF component and the rising band at 3450 cm^{-1} the red shift can be used to give the acid strength, Δv_{OH} = - 264cm^{-1}.

3.1.3 XRD Powder diffraction

Below (Figure 27) are the XRD plots of the two catalysts used.

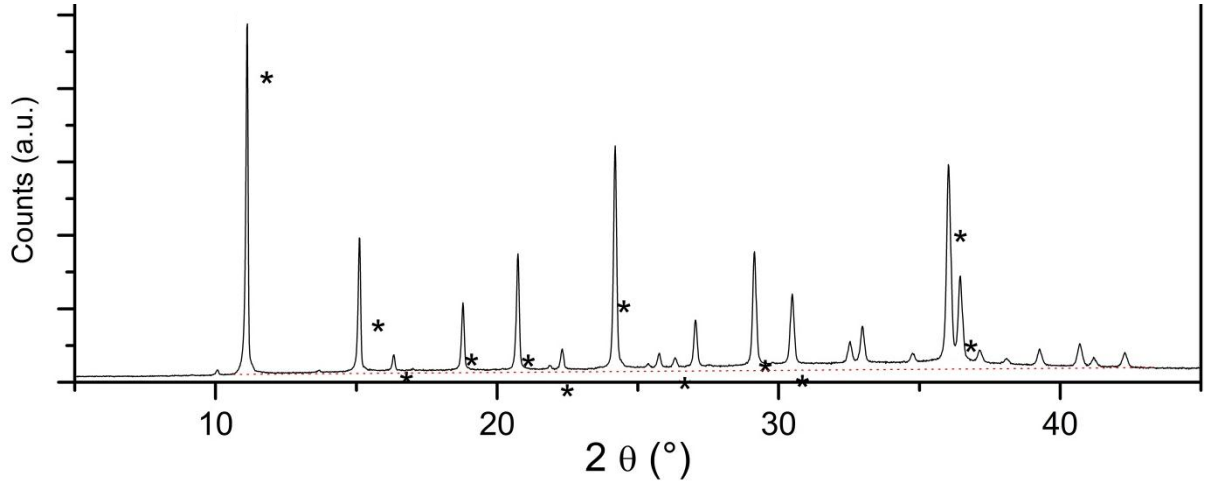

Figure 27. XRD patterns of the SAPO-34 after calcination

The asterisks indicate peaks characteristic for the CHA material, as reported by the International Zeolite Association.[104] The peak around 10° 2Θ is probably due to the use of this specific instrument instead of a zeolite phase.[77] The SAPO-34 shows to have CHA as crystalline phase; however, it does show a small amorphous phase between 25 – 40°. It is known that SAPO-34 is a more sensitive to water vapor than e. g. the zeolite SSZ-13 so this is in line with these findings. An older (over a month old) and fresh sample (from Figure 27) are compared in Figure 28. The intesitiy of peaks decrease and the baseline responsible for the amorphous phase increases. This underlines the importance to use fresh H-SAPO-34 and store it in a vial with parafilm.

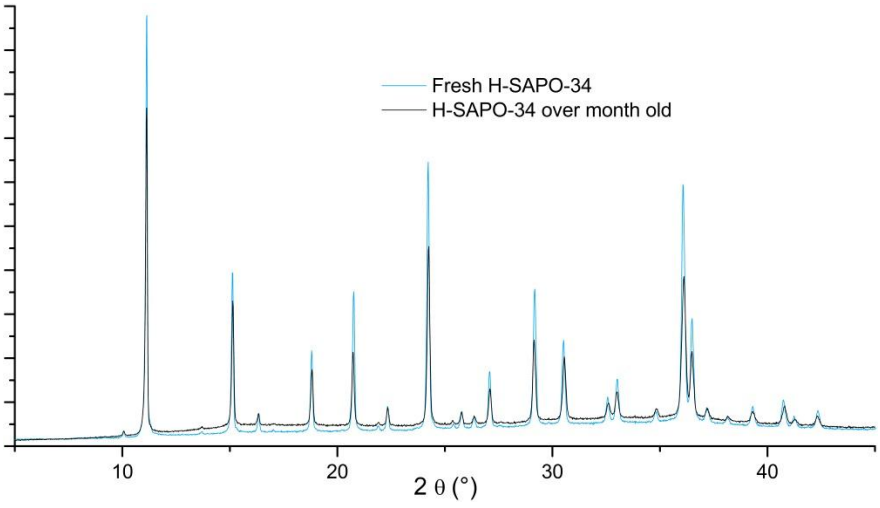

Figure 28. XRD diffractograms H-SAPO-34 catalyst a few hours (turquoise) and a month after calcination (black). Intensity representing the CHA framework lose intensity while the amorphous phase increases over time

3.2 Effect of concentration

The following section shows the results obtained studying different amounts of %Me with two different space velocities (WHSV = 0.3 g/(g.h) and 4 g/(g.h)).

3.2.1 Operando UV-Vis

To understand the molecular influence of water, it is important to make the diluting compounds nature the only variable in measurements. Thus, it is relevant beforehand to understand the effect of the methanol concentration (%Me) on the MTO reaction. To do so, a series of experiments was done with two different WHSV and varying %Me. A stable flow of methanol (2 mL/min, WHSV = 0.3 g/(g.h) or 10 mL/min, WHSV = 4 g/(g.h)) was diluted with increasing amounts to give information about the influence of %Me. For WHSV = 0.3 g/(g.h) methanol concentrations of 0.3 %Me, 1 %Me and 5 %Me were measured. For WHSV = 4 g/(g/h) methanol concentrations of 2 %Me and 14 %Me were measured.

Below are the results for WHSV = 0.3 g/(g.h), showing the conversion and selectivity measurements on the left and corresponding UV-Vis spectra on the right.

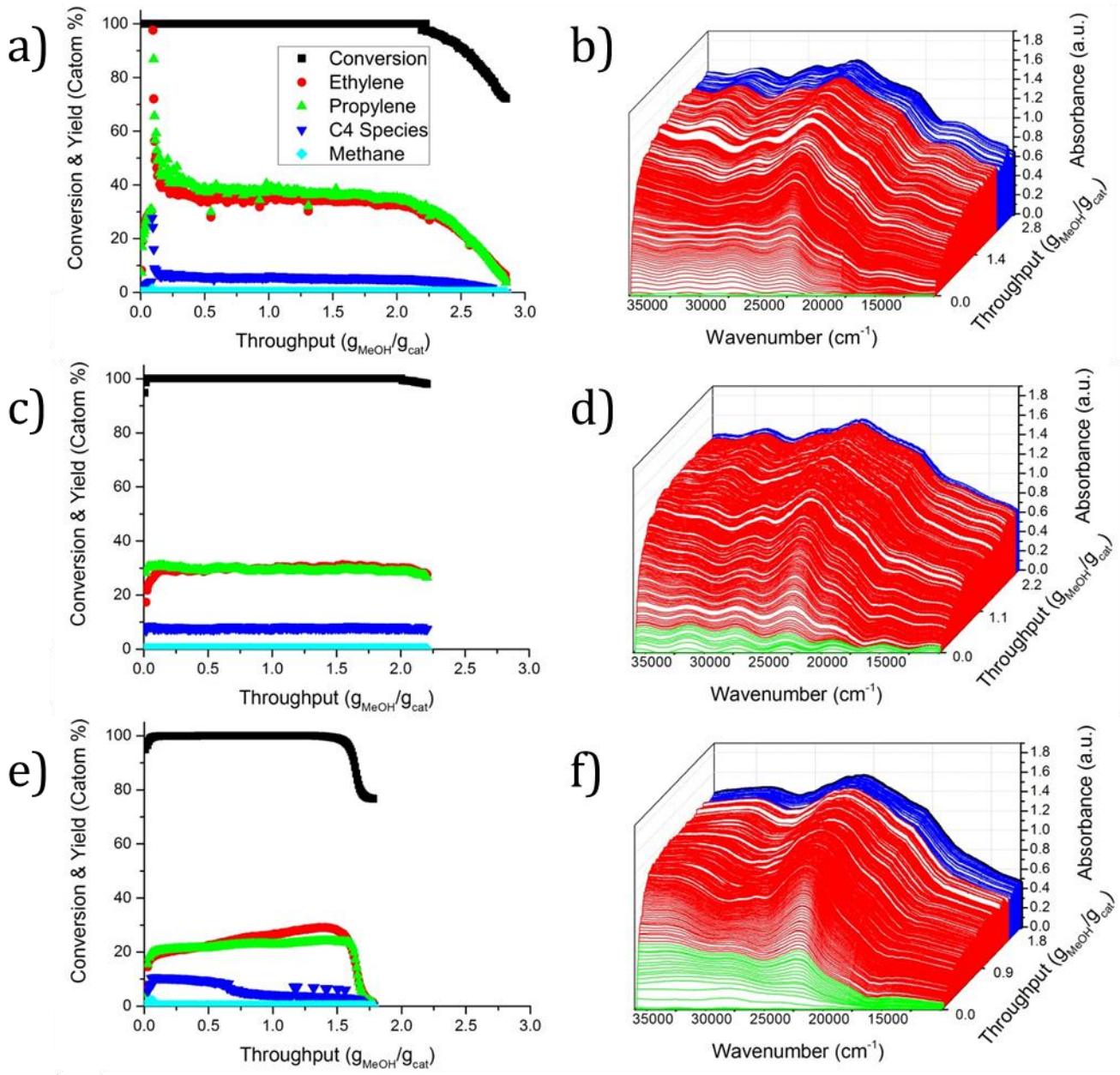

Figure 29. Operando UV-Vis results for different concentration of methanol (%Me) under WHSV = 0.3 g/(g.h). Left spectra show methanol conversion and product selectivity per carbon atom; a) 0.3 %Me, c) 1 %Me & e) 5 %Me. Right show the UV-Vis recorded over time, indicating the period in which recorded (IP, AP, DP) with the corresponding color for the different concentrations; b) 0.3 %Me, d) 1 %Me & f) 5 %Me. Note that due to technical difficulties the deactivation period of d) 1%Me wasn't recorded.

Table 2. Rough selectivity of the major products during the active period

Concentration	Ethylene (%)	Propylene (%)	C_4 (%)	Methane (%)
0.3 %Me	34	38	6	0
1 %Me	30	30	8	1
5 %Me	19-31	21-24	10-3	2-0

The left plots in Figure 29 show the selectivity. Averages during the active period are given in Table 2. Ethylene and propylene seem to decrease with increasing concentration. C_4 species and methane are increasing slightly. However, an interesting observation is the selectivity at 5 %Me. The ethylene and propylene selectivity increases over methanol throughput until the catalyst deactivates, while C_4 species and methane seems to show an opposite trend.

Table 3. Periods of reaction compared for different concentration of methanol. The values for periods are defined as gram of methanol converted per gram of catalyst (g_{MeOH}/g_{cat})

Concentration	Induction Period	Active Period	Deactivation Period
0.3 %Me	0.01	2.23	0.62
1 %Me	0.02	2.08	n.a.
5 %Me	0.05	1.45	0.28

When we calculate the amount of converted methanol per gram catalyst per period, we can define the periods as in Table 3. This gives us an indication about the lifetime of the catalyst. Since we're using different methanol concentrations, time is not representative for the catalyst lifetime as higher concentrations obviously convert more methanol in the same timeframe. While the IP seems to increase, both AP and DP decrease for higher %Me.

The UV-vis spectra (Figure 29b, d & f) show strong interference patterns. This makes it difficult to examine specific bands of spectra. Besides, Figure 29d is incomplete since it misses an amount of spectra for the DP. Figure 29b & f do show similar spectra at the end of the reaction though (black spectra, see them also combined in Appendix B, page 66). The experiments were repeated at higher WHSV = 4g/(g.h) (similar to the reaction conditions used for further experiments) as shown in Figure 30.

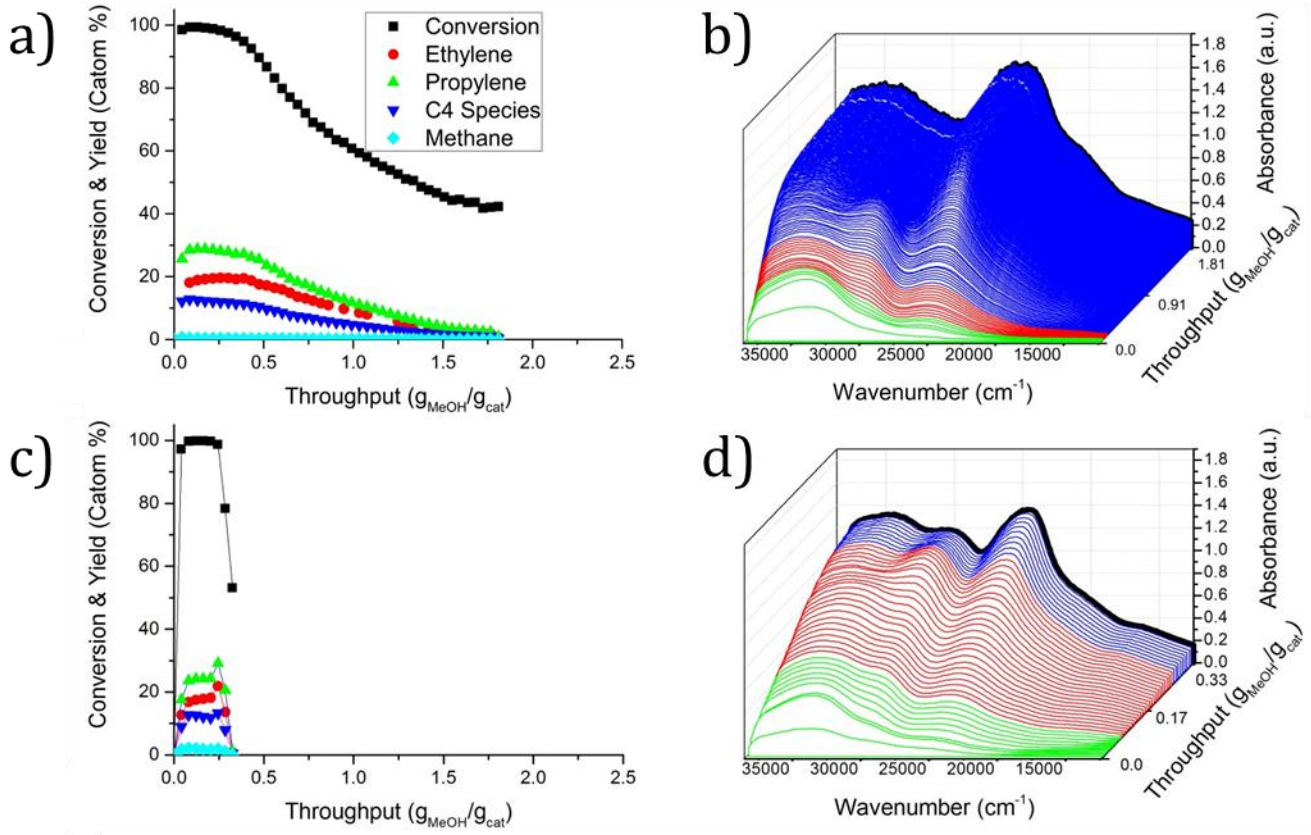

Figure 30. Operando UV-Vis results for 2 %Me (a, b) and 14 %Me (c, d) under WHSV = 4 g/(g.h). a) & c) show methanol conversion and product selectivity per carbon atom. b) & d) show the UV-Vis recorded over time, indicating the period in which recorded (IP, AP, DP) with the corresponding color.

Table 4. Rough selectivity of the major products during the active period

Concentration	Ethylene (%)	Propylene (%)	C_4 (%)	Methane (%)
2 %Me	20	29	13	0
14 %Me	18	24	12	1

Plots Figure 30a & c and Table 4 show the change in selectivity. Again, there seems to be a decrease in ethylene and propylene selectivity. C_4 species and methane selectivity are hardly influenced by concentration with this WHSV. The loss in light olefin selectivity must induce an increase for other products, however this is not observed from the GC-monitored species. A possible explanation for this loss is the rapid formation of deactivating species, consuming more MeOH. Therefore the selectivity for products becomes smaller while the catalyst is activated more rapidly.

When we look at the plots, we can see that at lower concentration the selectivity is constant before decreasing due to deactivation. At higher concentration though, the selectivity of ethylene and propylene seems to be increasing while C_4 species are decreasing. This is a similar observation as for WHSV = 0.3 g/(g.h), although the observation is less pronounced due to the short active time.

Multiplying the yield with methanol put through gives the actual yield during the reaction. It is obvious that a higher catalyst lifetime therefore leads to a higher reaction yield, for both WHSV.

Table 5. Periods of reaction compared for different concentration of methanol. The values for periods are defined as gram of methanol converted per gram of catalyst (g_{MeOH}/g_{cat})

Concentration	Induction Period	Active Period	Deactivation Period
2 %	0.04	0.22	1.55
14 %	0.04	0.16	0.08

As can be seen in Table 5, the difference in total throughput between the two concentrations is large. Although the IP and AP are still of similar order, the DP is 19 times larger. The UV-Vis recordings show no interference as before. It is also clear the end spectra (black, see also Appendix B, page 66) is lower for higher %Me. However, to obtain additional information about these UV-Vis spectra, NNMF-analysis is necessary.

3.2.2 NNMF analysis

Below are the results obtained from the Operando plots after NNMF analysis. The left plots will show the eigenspectra and the right the corresponding kinetic profiles.

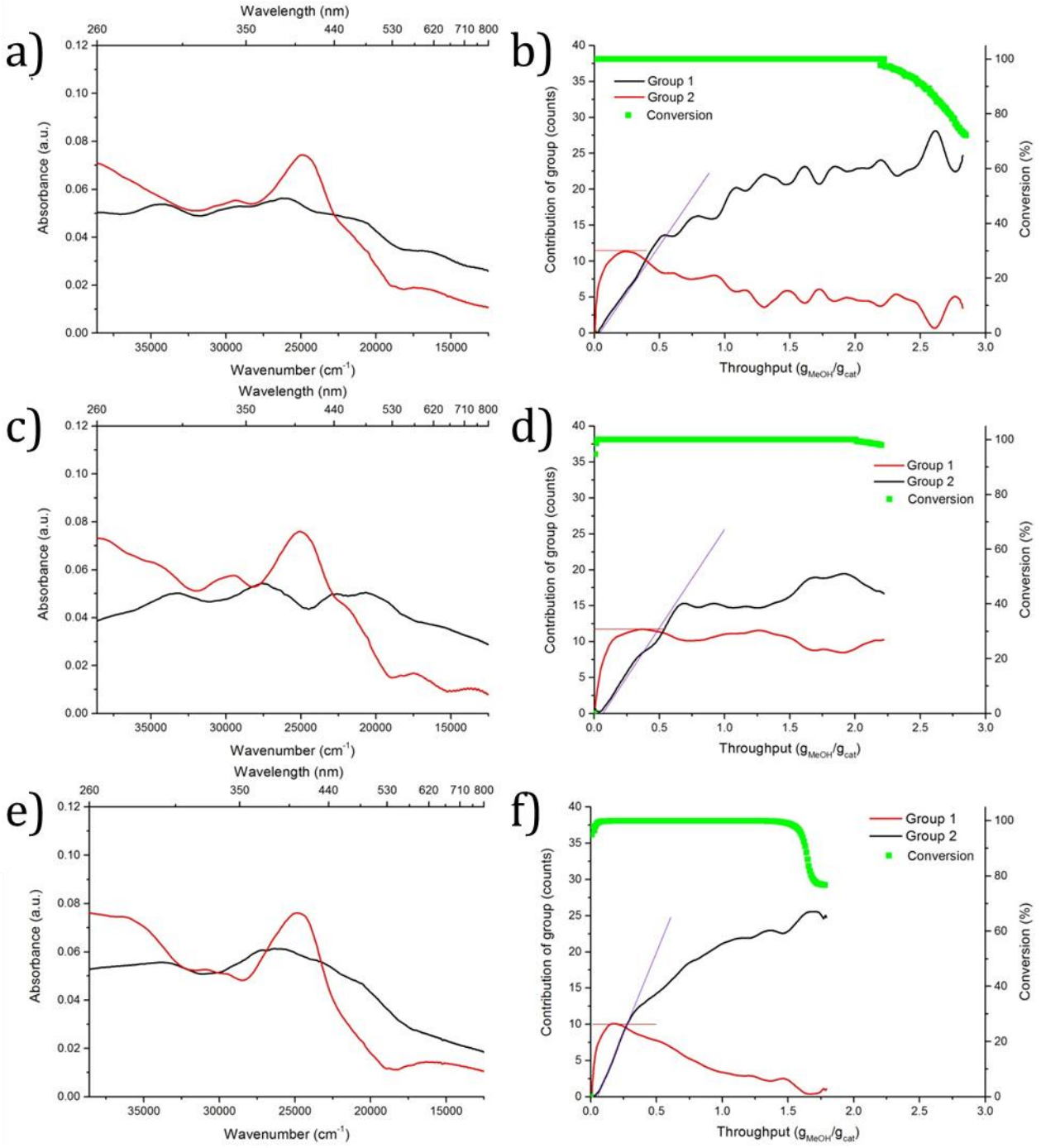

Figure 31. NNMF profiles of 0.3 %Me (a, b), 1 %Me (c, d) and 5 %Me (e, f) under WHSV = 0.3 g/(g.h). Figures a, c & e show the eigenspectra representing the bands forming a group, while the kinetic profiles b, d & f give the contribution of this group over time. Note again that for 1 %Me the deactivation period was not recorded (influencing c & d)

When we look at the eigenspectra for all different concentrations with WHSV = 0.3 g/(g.h), we can see rather similar eigenspectra. Looking at the kinetic profile of the groups, it becomes clear that red must represent the active species, since their contribution increases rapidly at the start of the reaction and then slowly decreases over methanol throughput. The black eigenspectra represent the deactivating species, since the kinetic profile shows a square root-like elapse over methanol throughput.

In the eigenspectra of active species, there is a dominant band present for all different concentrations at 24910 cm-1 / 402 nm. This band represents HMB carbocations, which are found to be key intermediates in the MTO mechanisms. [62] A smaller band is observed around 30000 cm^{-1} / 333 nm. This band might represent dienylic species. [77], [105] Although a band for monoenylic species is expected around 35000 cm^{-1} / 286 nm, the eigenspectra of WHSV = 0.3 g/(g.h) show no maximum at this specific energy. This might be due to the interference in the original UV-Vis spectra. A shoulder band can be distinguished around 22000 cm^{-1} / 455 nm. This shoulder represents methylated naphthalene carbocations. [10], [106] The last band observed is around 16000 cm^{-1} / 625 nm and is found to be phenanthrene/anthracene carbocations. [10], [106]

The eigenspectra of deactivating species shows a broad band for 0.3 %Me and 5 %Me centered around 25000 cm^{-1} / 400 nm, while 1 %Me seems to have two bands. [78], [105], [107], [108] This is likely because 1 %Me was aborted before completely deactivated, therefore not fully converting to the larger neutral polyaromatics (which may be found ~25000 cm^{-1}). It could also be influenced by the interference. Although the profiles might be fluctuating due to the interference in the original UV-Vis, we can obtain useful information by looking at the maxima and slopes as drawn in Figure 31. The maxima of the active species contribution tell us the amount of species active at its peak. With increasing concentration, this maximum seems to decrease as can be seen in Table 6. For the slopes drawn, we might say this gives us the rate of formation of species deactivating in nature. This rate is increasing with higher concentrations.

Table 6. Maxima for active species and slopes for deactivating species from kinetic profiles in Figure 31b, d & f.

Concentration	**Maxima (counts)**	**Slope (counts/{g_{MeOH}/g_{cat}})**
0.3 %	11.4	26.5
1 %	11.8	27.2
5 %	10.0	44.4

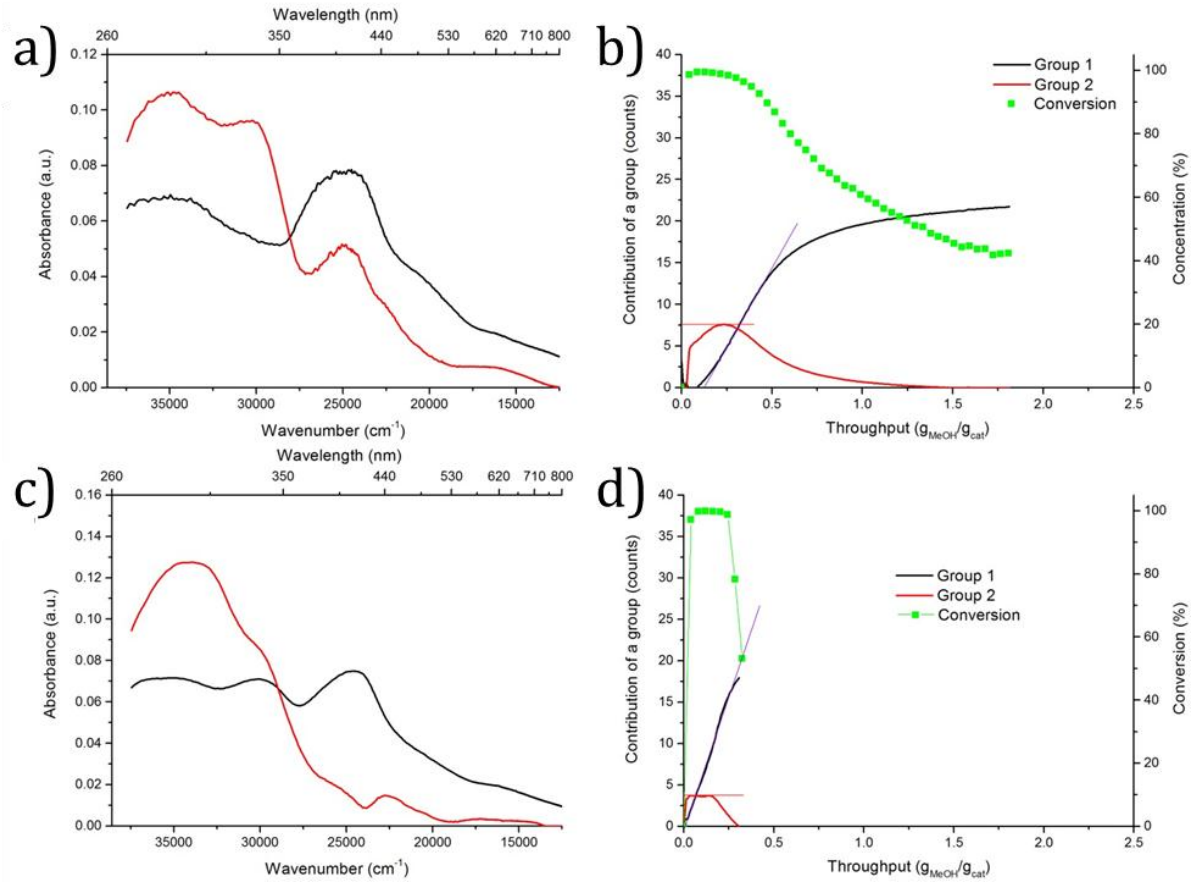

Figure 32. NNMF profiles of 2 %Me (a, b) and 14 %Me (c, d) under WHSV = 4 g/(g.h). Figures a & c show the eigenspectra representing the bands forming a group, while the kinetic profiles b & d give the contribution of this group over time.

The NNMF analysis for WHSV = 4g/(g.h) shows major differences both in nature of eigenspectra and kinetic profiles. When looking at the eigenspectra of 2 %Me (Figure 32a) we can see 4 clear bands for the active species. The first band (~35000 cm^{-1} / 286 nm) represents monoenylic species, this time clearly represented, while the second band (30000 cm^{-1} / 333 nm) accounts for dienylic species as described before. The third band represents the HMB carbocations band as explained before. Both methylated naphthalenic (22000 cm^{-1} / 455 nm) and phenanthrenic/anthracenic (16000 cm^{-1} / 625 nm) carbocations as described before are observed. The 14 %Me (Figure 32c) shows the monoenylic band but the dienylic band seems to be decreased to only a shoulder. Besides, the HMB carbocations band seems to have disappeared almost completely. The phenanthrene/anthracene carbocations band is decreased in intensity as well while methylated naphthalene carbocations show relatively high intensity. The deactivating species both show the broader neutral polyaromatics band (~ 25000 cm^{-1}) and a small broad band might be identified representing neutral benzenes (35000 cm^{-1} / 286 nm) [77], [105], [109] The kinetic profiles show similarities with the lower WHSV. The maximum contribution of active species decreases for an increased concentration while the rate of formation of deactivating species increases as shown in Table 7.

Table 7. Maxima for active species and slopes for deactivating species from kinetic profiles in Figure 32b & d.

Concentration	Maxima (counts)	Slope (counts/{g_{MeOH}/g_{cat}})
2 %	7.6	38.4
14 %	3.8	64.4

Discussion on methanol concentration

When looking at the averaged selectivities for the different %Me (Table 2 & 4), we noticed a constant, slightly increasing C_4 species and methane selectivity. The ethylene and propylene selectivity decreased for increasing %Me. This is an observation often made by earlier studies "adding" water. Another noticeable effect (especially for the high %Me) is the gradual decline of ethylene and propylene selectivity in one experiment, while the C_4 species selectivity acts opposite. Possibly, this is due dimerization reactions, which are initiated more easily with higher methanol concentration. Then, while the reaction elapses, stronger acid sites get occupied by larger active or deactivating species and direct dimerization becomes difficult, thus decreasing the C_4 species selectivity and increasing the propylene and (greatly) ethylene selectivity.

Considering the throughput values from Table 3 & Table 5, several results can be explained. Analyzing the IP, an increase is observed with higher concentrations with WHSV = 0.3 g/(g.h). This is counter-intuitive, since one might expect the catalyst to perform faster with higher concentrations. However, these concentrations are inverse proportional to the flow speed, since lower concentrations are achieved by adding diluent and thus increasing the total flow. Therefore, the increase in IP might be due to the delay of the products reaching GC, while GC recordings are slow compared to the UV-Vis. For higher flow speeds / total flow, this problem becomes more negligible since the measured flow at the reactor reaches the GC rapidly. Since the experiments at WHSV = 4 g/(g.h) have higher total flows, the decreased IP is not observed here. The AP shows a decrease in converted methanol with an increase in concentration. Although the 1 %Me for WHSV = 0.3 g/(g.h) (Figure 29d) has no DP recorded, this trend is observable for the DP as well. For WHSV = 0.3 g/(g.h) we saw a small increase in total throughput comparing 0.3 %Me with 5 %Me. For WHSV = 4 g/(g.h) the difference in concentration for 2 %Me with 14 %Me is smaller, still the difference in total throughput is way higher. We may conclude from this that increased WHSV amplifies the differences found, probably because the catalyst feels more stress under a higher space velocity. The effect of concentration can be thought of to be somewhat similar to the results of water from Wondergem [110]. When considering the concentration of methanol to be the probability of methanol molecules interacting with the active sites of zeotypes cages, the results can be explained. When methanol flows over the catalyst bed, it will react on an active site in the cages of the zeotype. However, when the concentration of methanol is high, more methanol might react in the outer cages of the particle. Since this initiates the formation of large coke species (which deactivate the cage or block the pore) at a high rate, it's assumable that a higher concentration leads to

deactivation of the outer part of the zeotype particle. As a result, the inner parts are almost unused before the catalyst is defined as deactivated (see Figure 33).

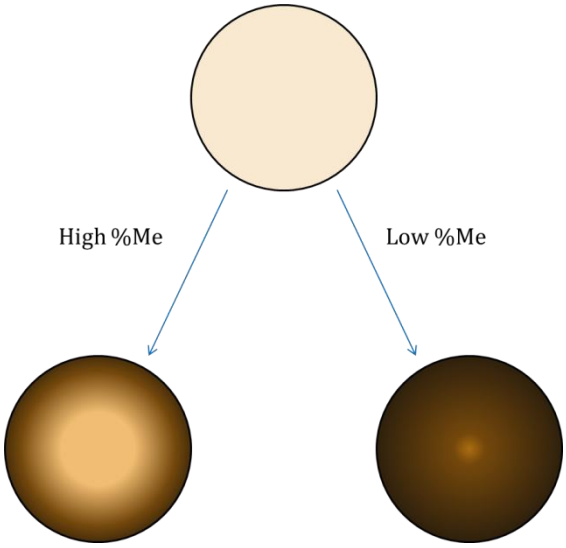

Figure 33. Schematic representation of the influence of %Me on the coke distribution and therefore catalyst lifetime

This explanation can also be strengthened by looking at the color of the different spent catalysts: it is clear that a higher concentration deactivates the catalyst before all cages are optimally used and therefore obtain a lighter color (see Figure 34).

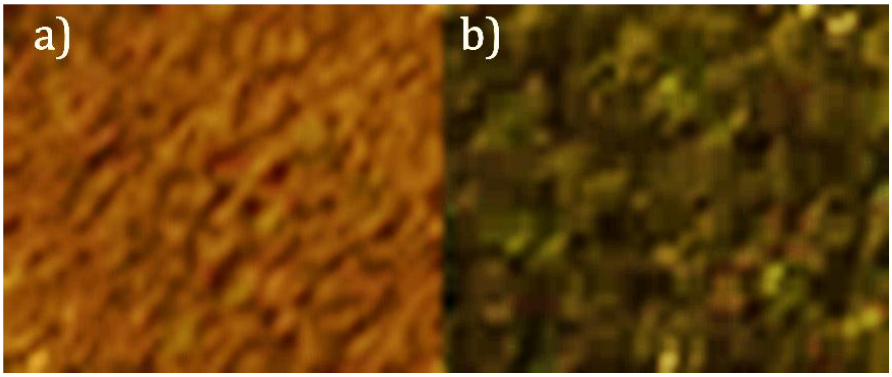

Figure 34. Spent catalyst samples of 5 %Me (a) and 0.3 %Me (b) (brightness + 60%)

When looking at the UV-Vis data to give us information about the nature of the HCP species, we must first keep in mind that there seems to be a strong interference in the spectra for WHSV = 0.3 g/(g.h). Although some bands are distinguishable, the overall features are hard to determine due to the interference and similarity in the spectra. Spectra for WHSV = 4 g/(g.h) are clearer and show the overall intensity of the higher concentration to be higher at the end of the reaction. This is another effect of the higher amount of species present in catalysts which have performed under a lower concentration of methanol. To get a clearer view on active species and kinetics we must focus

on the NNMF analysis. Using NNMF (Figure 31 & Figure 32) to look at the kinetic profiles, a decreased contribution of active species and increased rate of formation of deactivating species are observed for higher concentrations. These observations are perfectly in line with the explanation from Figure 33; a lower concentration lowers the rate of formation of deactivating species and therefore the contribution of active species becomes larger. A higher concentration forms deactivating species more rapidly (in the outer pores) deactivating the catalyst and thus keeping the contribution of active species lower. Besides, for WHSV = 4 g/(g.h) the catalyst was activated so quickly (Figure 32) with high %Me that more complicated active species were hardly formed in inner pores. In the end, we have two relevant observations i.e., increased olefin yield and longer active time, which are in literature ascribed to the effect of water. [86], [87], [89] This is due to the diffusivity of methanol. Apparently, a lower concentration of methanol makes the probability of interaction in outer pores smaller, creating a more homogeneous distribution of species throughout the particle.

3.3 *Effect of water*

The following section will focus on the effect of water. Since concentration focusses on diluting the methanol flow, all experiments in upcoming part will have a constant concentration (2 %Me) and space velocity (WHSV = 4 g/(g.h)). It's important to keep in mind that the *nature of diluent* (He/N_2 with or without water) is the only variable.

3.3.1 *Operando UV-Vis*

Below are the results of the operando UV-Vis experiments, first focusing on the conversion and selectivity results, then on the corresponding UV-Vis plots.

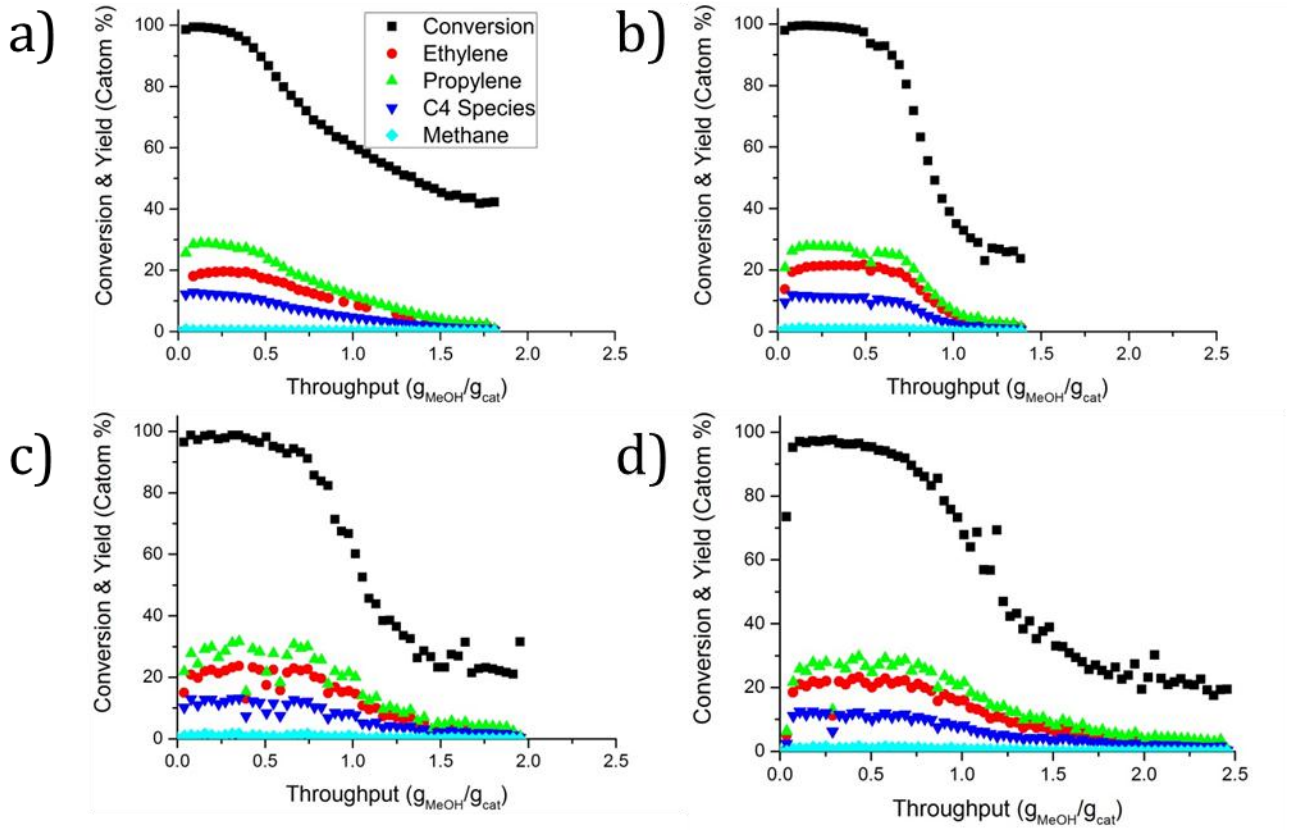

Figure 35. Conversions and product selectivies during the methanol to olefins reaction on SAPO-34 from the Operando UV-Vis experiments for methanol/water = 1/0 (a), 1/4 (b), 1/6 (c) and 1/10 (d)

The selectivity of the different Me/Wa in Figure 35 shows no differences. Noticable are the data points being more scattered for higher water contents. This might be due to some water condensation in the setup and therefore some fluctuations in pressure and GC measurements. The selectivity is deliberately plotted with data points instead of lines, to make analysis clearer.

Table 8. Periods of reaction compared for methanol/water ratios.
The values for periods are defined as gram of methanol converted per gram of catalyst (g_{MeOH}/g_{cat})

Me/Wa ratio	Induction Period	Active Period	Deactivation Period	Total reaction (IP + AP + DP)
1/0	0.04	0.22	1.55	1.81
1/4	0.08	0.37	0.94	1.39
1/6	0.08	0.47	1.41	1.96
1/10	0.11	0.22	2.13	2.46

The different periods of reaction are given in Table 8. The IP does increase with more water content. However, the AP and DP show no clear trend. Looking at the total reaction throughput, we might say that this increases with water content but by using these definitions of the different periods we can't find a trend. Multiplying the yield with methanol put through and thus giving us the yield over reactions as in Figure 36 shows a more clear increase.

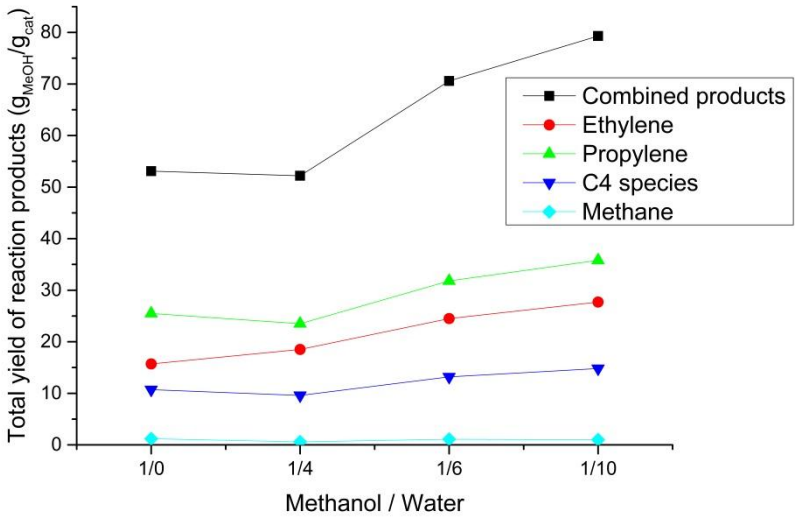

Figure 36. Yield obtained during the complete performed reaction, multiplying selectivity with methanol throughput. The x-axis shows the different methanol/water ratios.

Below are the UV-vis plots, part of the Operando measurements together with Figure 35.

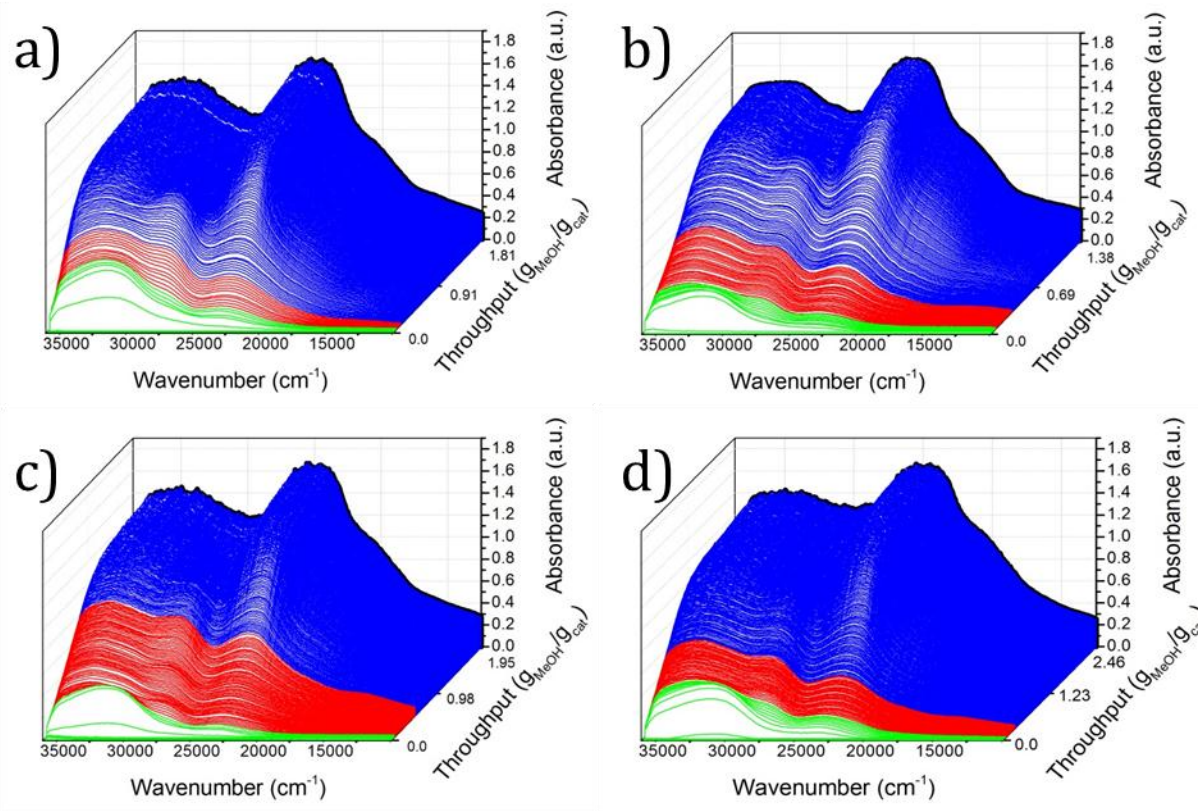

Figure 37. UV-Vis plots corresponding to the conversions and product selectivies measurements in Figure 35 for methanol/water = 1/0 (A), 1/4 (B), 1/6 (C) and 1/10 (D)

The UV-Vis spectra from Figure 37 look similar on first sight. A noticeable similarity is the total absorption at the end of the reaction (black spectra, see also Appendix B on page 66). The large HMB carbocations + neutral polyaromatic band around 25000 cm^{-1} ends at 1.7 a.u. for all Me/Wa ratios and the mono- and dienylic species seem to be similar as well. However, although the absorbance at the end might be similar, the development of bands over time could be influenced. This can be observed from the NNMF analysis.

3.3.2 NNMF Analysis

On the next page are the results for the NNMF analysis of the different Me/Wa ratios. Left show the eigenspectra, with the corresponding kinetic profiles on the right. Water content increases from top to bottom.

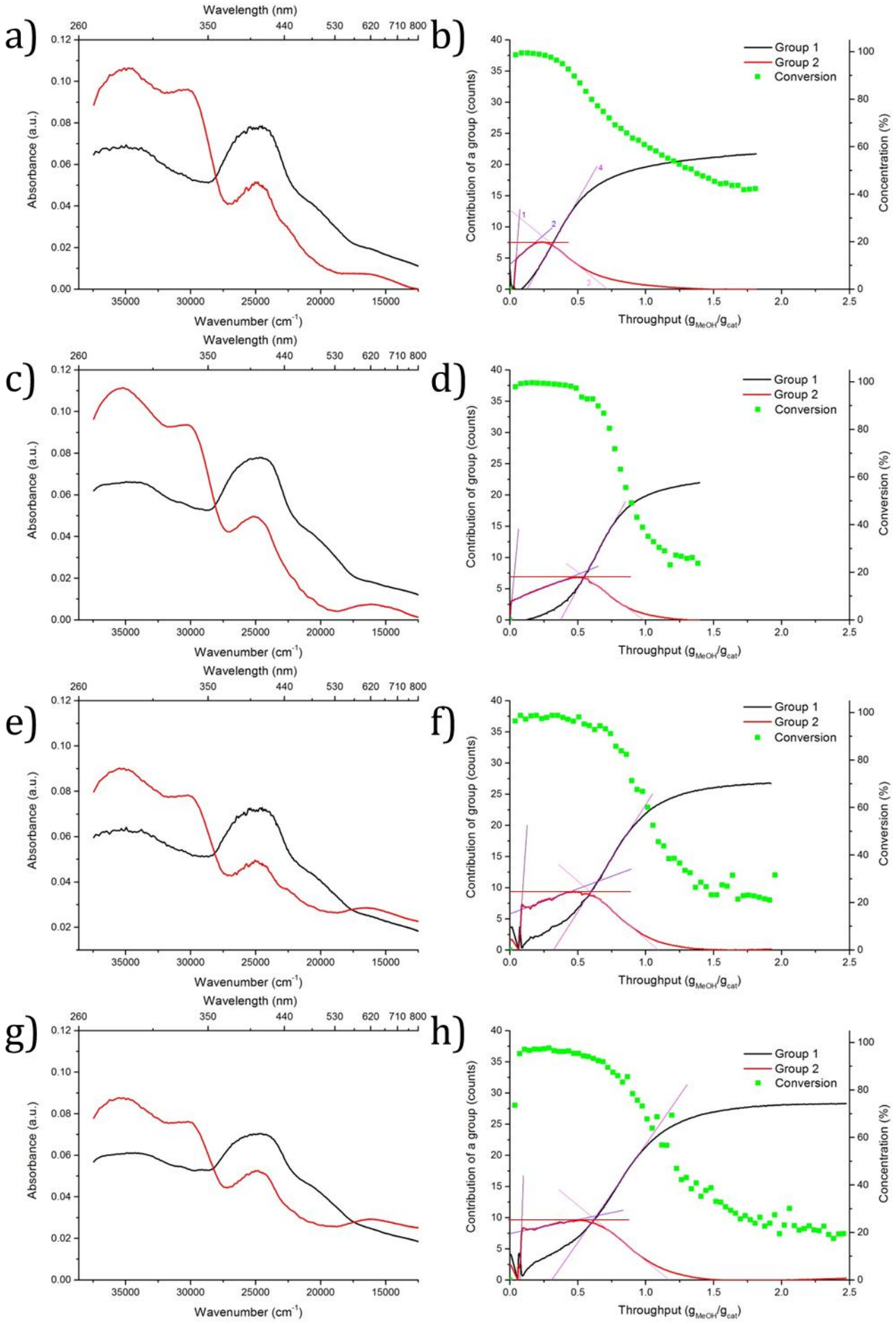

Figure 38. Eigenspectra (a, c, e, g) and corresponding kinetic profiles (b, d, f, h) of different methanol / water ratios; 1/0 (a,b), 1/4 (c, d), 1/6 (e,f) and 1/10 (g, h)

The eigenspectra in Figure 38 show bands seen in previous results; the monoenylic (~35000 cm^{-1} / 286 nm), dienylic (~30000 cm^{-1} / 333 nm), HMB carbocations (25000 cm^{-1} / 400 nm) and phenanthrene/anthracene carbocationic (15000 – 16000 cm^{-1} / 666 nm) species are present in the active group. In the deactivating group, the not-so-intense band representing neutral benzenes (~35000 cm^{-1} / 286 nm) and the dominating band representing polyaromatics (~25000 cm^{-1} / 400 nm) are present. A shift in intensities is observed with increasing water content. Both mono- and dienylic species decrease in intensity as active species with increasing water content. On the contrary, phenanthrene and anthracene carbocationic species increase in intensity with more water present in the feed. The deactivating species show no significant changes. The kinetic profiles show interesting features. Looking at the maximum contributions of active species, we can see that the maximum contribution of active species increases for the two higher water ratios. As seen in Figure 38, slopes can be assigned to different components of the profiles (see Table 9).

Table 9. Slopes from NNMF kinetic profiles. The values are given in $\{counts/(g_{MeOH}/g_{cat})\}$

Me / Wa ratio	Slope 1	Slope 2	Slope 3	Slope 4
1/0	322	18.9	-17.9	38.0
1/4	243	8.58	-15.9	39.6
1/6	286	8.11	-18.8	34.4
1/10	335	4.52	-19.1	31.4

These slopes give us information about the rates of formation or transformation of species, as shown in Figure 39. *Note that the exact nature of species is not known, but groups of compounds are shown as representatives.*

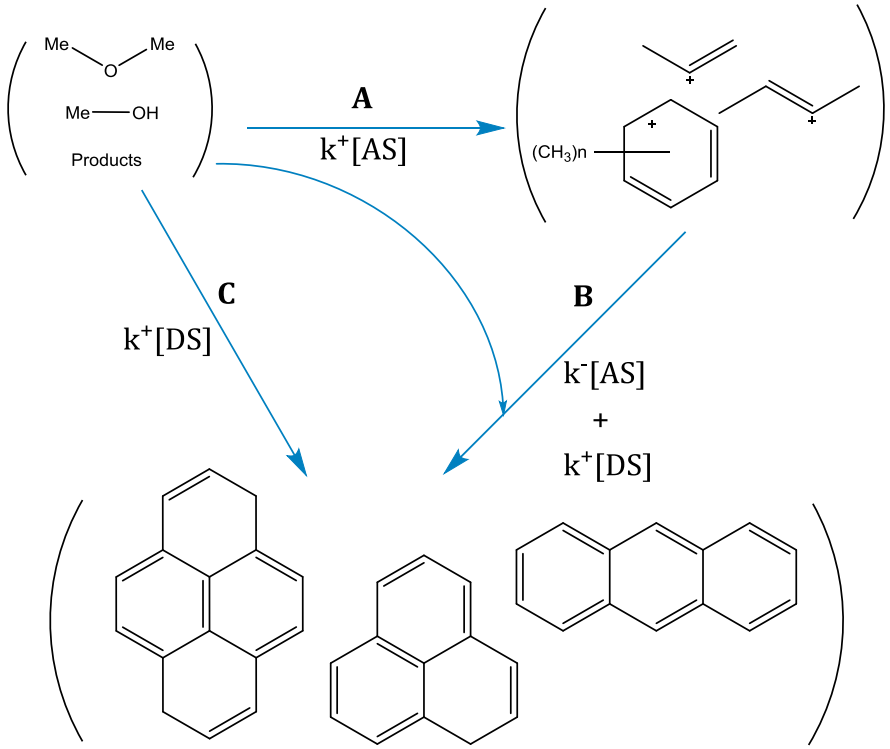

Figure 39. Scheme representing broad formation steps of 2 NNMF components. Compounds shown are only *representative* to the group and not proved to be present in the HCP experimentally in this research

The scheme in Figure 39 gives us the opportunity to tell something about the influence of water on the broad reaction steps in the MTO reaction.

- Slope 1 contributes to scheme-step **A**
- Slope 2 contributes to scheme-step **A**
- Slope 3 contributes to scheme-step **B**
- Slope 4 contributes to scheme-step **B** and **C**

Slope 1 accounts for the *formation of active species.*
We could state slope 1 is representative singularly for the IP. Table 8 showed an increase in induction period with increasing water content. We might expect the $k^{+}[AP]$ during the induction period, which is slope 1, to be decreasing. However, the slopes are so steep, that it is hard to assign them perfectly and the error is probably significant. We might say the slopes look similar, but no hard statements can be made about these values.

Slope 2 accounts for the *formation of active species (after the IP).*
This slope decreases with increasing water content as can be seen in Table 8.

Slope 3 accounts for the *transformation (and thus loss) of active species.*
Slope 3 is rather constant. The loss of active species can be seen as a gain in deactivating species, since active species transform to deactivating species retarding the catalytic performance. Water does not have an influence on this transformation of active to deactivating species.

Slope 4 accounts for the *formation of deactivating species.*
The formation of active species as described by slope 4 can be represented by two reactions. First, it is possible to have direct formation of deactivating species from reagents / products, so light olefins, methanol and DME. The second contribution is the transformation of active species to deactivating species as described by Slope 3. Water decreases the slope, meaning the formation of species deactivating the catalyst.

3.3.3 TGA Analysis

The TGA from the spent catalysts from the different Me / Wa ratio are shown in Figure 40.

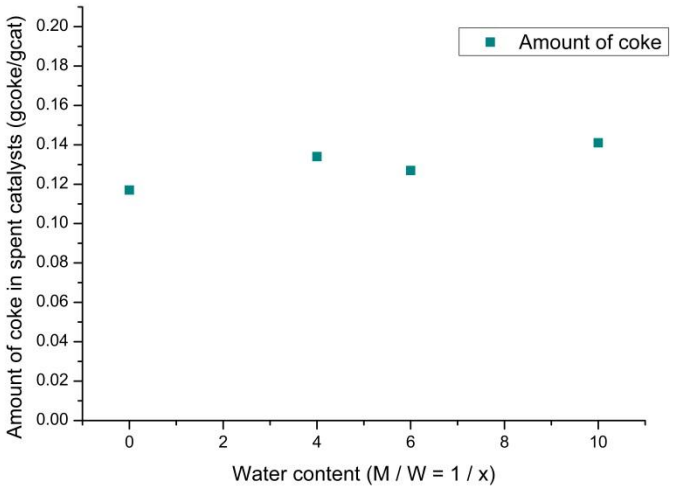

Figure 40. The amount of coke per gram of spent catalyst obtained after TGA analysis.

The differences in coke are small. The paper by Borodina et al. claimed an increase for formed coke with increasing temperature. This increase was an increase of 0.07 g/g_{cat}. [77] The maximum difference between the TGA from our analysis was 0.022 g/g_{cat}. Comparing these values to the UV-Vis spectra of the spent catalyst (Appendix B, Figure 47) show a similar small increase.

Discussion on the effect of water

The catalytic performance was influenced by water in the feed. It was clear that increased water content increases the IP. Both AP and DP showed no clear trend whatsoever. The selectivity towards olefins or specific C_n species wasn't influenced. The total amount of product yield was higher for larger water ratios. This assumes water increases product output, possibly by stabilizing intermediates from reacting with formed products.

The UV-Vis showed no differences at first glance. Bands, intensities and end spectra were all similar. However, NNMF gave a more in-depth look. As the active species indicated a shift in intensity of smaller (mono- and di-) enylic species to larger polyaromatics carbocations, water seems to influence the nature of actively contributing species. It is questionable that phenanthrene and anthracene carbocations act as co-catalyst since their large size compared to the cavities of SAPO-34, qualifies them almost exclusively as coke. It might be so that water stabilizes these carbocations from further methylation, thus keeping them from being 'deactivating' whilst they are not contributing to the actual product formation. However, using the given data, this can't be elaborated on further. Since the eigenspectra of deactivating species remained similar for all water content, the change in active species is purely a shift in contribution of active species. There are no species becoming active or deactivating while first opposite of nature. This makes the explanation of the intensity shift for active species more plausible.

When looking at the kinetic profiles, we observed an increase in contribution for active species for higher water ratios. This is in line with the higher yield, concluded from the catalytic performance tests. Referring back to Figure 38 and Table 9, it becomes clear that k+[AS] and k+[DS] are affected by water. More interestingly, slope 3, which is only slope representative for k-[AS], is unaffected. All steps, A, B & C are influenced by water. This leads to state that water is directly influencing the reactivity of the Reagents-group, consisting of MeOH, DME and formed products like light olefins. The transformation of active to deactivating species, so processes like cyclization and reduction of carbocations, is not influenced by water. The reaction of active species with methanol, DME and/or olefins is slowed down, as is the direct formation of active or deactivating species by methanol, DME and/or olefins. This is perfectly in line with the higher total yield and maximum contribution of active species.

Since the UV-Vis spectra and TGA analysis showed no difference and the AP and total throughput showed no clear increase for increasing water content, we could speculate this observation to be unrelated to Brønsted acid sites. If competitive adsorption between the methanol and water would be the cause of this reduced reactivity, the species would have a more homogenenous distribution of UV-Vis active polyaromatics and therefore a darker color / higher UV-Vis intensity. However, if we do call the increase in UV-Vis spectra and burned coke from TGA significant, it would an increase.

On the contrary, the decrease in Slope 2 from the NNMF analysis implies there is a retardation on the formation of active species and thus HCP. Additionally, the contribution of active species at its maximum increased for higher water contents. This means water *does* show competitive adsorption with methanol, forcing it to diffuse deeper into the zeolite particles and thus explaining the *slower* formation of active species and their *higher* contribution at its maximum. The total active time and similar UV-Vis spectra of spent catalysts might be explained by the reaction conditions. From the concentration experiments, it became clear the high concentration led to a decreased catalytic performance. For these water experiments, using the same conditions as the low concentration one, the catalyst might be optimally used without water, explaining why the increase in total amount of species in the spent catalyst is so small. This has as consequence that only the effect of water *during* the reaction can be observed, since all reactions will end in similar results, underlining the importance of operando characterization techniques.

To repeat and conclude, the influence of water on the reagents and products gives rise to several positive effects: a higher total yield of olefins, a higher contribution of active species and a slower formation of deactivating species. This can be explained by competitive adsorption between water and methanol.

3.4 Propylene feeding experiments

To gain insight into the effect of water on the formation of deactivating species from olefin products, operando measurements feeding only propylene and water were performed.

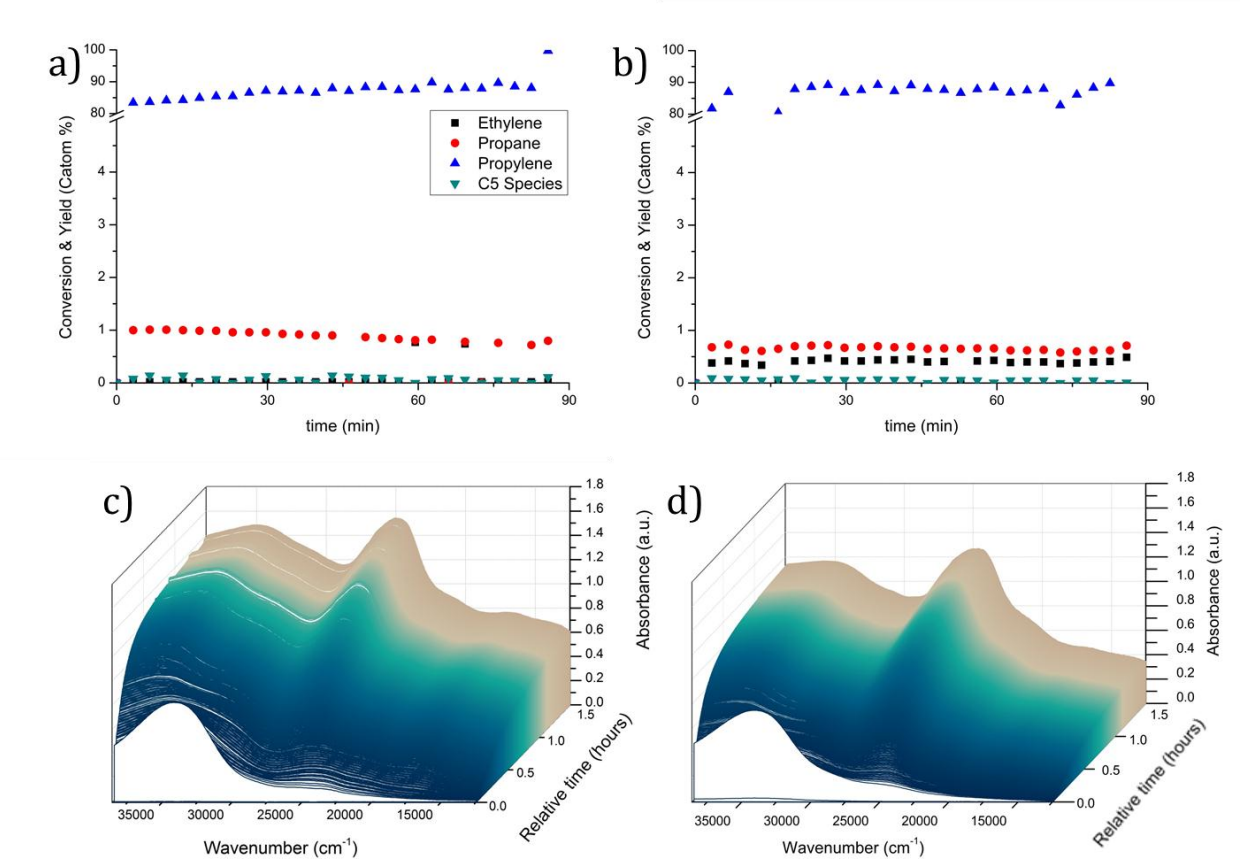

Figure 41. Propylene feeding over H-SAPO-34. The propylene / water 1/1 results are displayed in a) and c), while 1/9 results are shown in b) and d). Conversion and selectivity plots (a & b) show huge similarity, although ethylene formation increases slightly with the higher water content. UV-Vis spectra (b & d) show a clear difference in amount of absorbance (= species) at the end of the 1.5 hours run

When considering the conversion and selectivity plots from Figure 41a, propane and ethylene are the main products. The higher formation of propane when water is added in stoichiometric amounts clearly indicates the formation of more hydrogen deficient species, which are not observed in the chromatograms and most likely remains in the catalysts. This is also correlated by the UV-Vis measurements. First of all, the large band around 33000 cm^{-1}, probably monoenylic species, seems to be higher for the propylene / water = 1/1. Besides, the last spectra (in brown) has lower intensity for the 1/9 ratio, meaning a smaller amount of total species in the catalyst.

The plots after NNMF analysis on the UV-Vis spectra are shown in Figure 42.

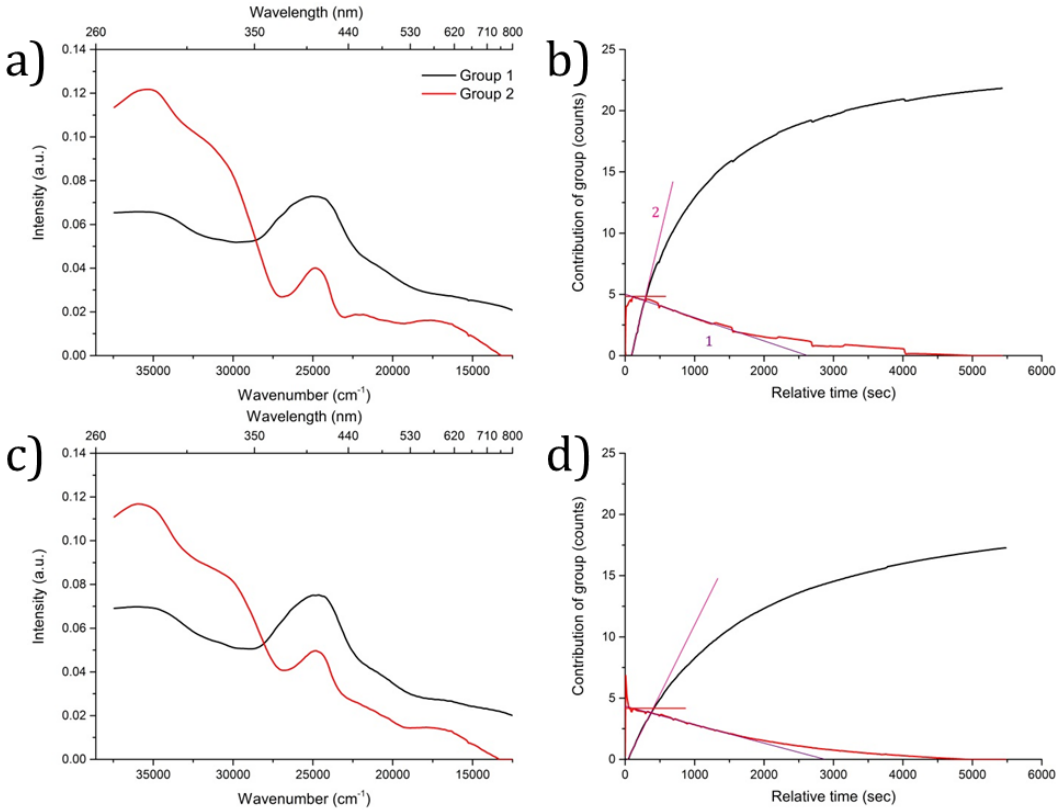

Figure 42. NNMF analysis of the UV-Vis spectra obtained from the propylene feeding experiments. Prop/water = 1/1 is represented by the upper eigenspectra and kinetic profile (a & b) while 1/9 by the lower (c & d). Slopes 1 and 2 are drawn together with the maximum contribution of Group 2 species

The obtained eigenspectra look similar to eigenspectra from earlier experiments. However, we can not state that above eigenspectra represent active species in the MTO reaction, since methanol wasn't used as reagent. This can be confirmed by considering the band around 25000 cm^{-1} / 400 nm. For the MTO experiments, this band represented HMB carbocationic species and has a maximum at 25000 cm^{-1} / 400 nm exact (i.e.; Figure 38). The band in Figure 42 has a maximum at 24824 cm^{-1} / 402 nm. This means the species responsible for this band are not HMB carbocations but rather methylated naphthalene carbocations. [10], [77], [106] Inspecting the slopes 1 and 2, the rate of disappearance of "active species" and formation of deactivating species are calculated. The rate of disappearance of active species seems to be unaffected by the addition of water. However, the rate of formation of deactivating species is clearly affected and decreases more than half when water is added in amounts higher than stoichiometric.

Table 10. Slopes from NNMF analysis kinetic profiles in Figure 42b & d. Values are in counts/sec

Slope	Prop / water = 1 / 1	Prop / water = 1/ 9
1	$1.9 *10^{-3}$	$1.5 *10^{-3}$
2	$24 *10^{-3}$	$11 *10^{-3}$

Discussion on the effect of water in propylene feeding experiments

To prove water is influencing the formation of deactivating species from the olefin products, propylene was fed to the catalyst with and without extra water. Assuming that we can define the bands from the NNMF analysis in a similar manner as for the water experiments (Figure 38) we see a difference in nature for the active species Not HMB carbocations but rather methylated naphthalene carbocations are active contributors to the propylene feeding reaction.

Additionally, the kinetic profiles support the theory that the reactivity of propylene is influenced by water. The conversion and selectivity plots in Figure 41 show that propylene has a modest reactivity under these condition. After the same amount of time, the total amount of coke species for the propylene / water = 1/9 ratio is lower. Slope 1, if it would be representative for active species in the MTO reaction, is unaffected by water, similar as described in Figure 39. Slope 2 decreases more than half when adding higher amounts of water. This result is similar to the decrease in slope 4 from Figure 38. In this propylene feeding experiment, it becomes clear that water has a retarding effect on the formation of deactivating species. The selectivity plots show propane selectivity is higher for stoichiometric amounts of water, implying the formation of more hydrogen deficient species. This is confirmed by the UV-Vis spectra and the kinetic profiles obtained from NNMF analysis on them.

Chapter 4 – Conclusion

In this research, operando UV-Vis has been used and analyzed thoroughly to elaborate on the influence of water on the methanol-to-olefins reaction catalyzed by H-SAPO-34. It was shown that methanol concentration influences the catalytic performance. A lower methanol concentration gives rise to a higher total active time, a higher olefin yield and improved light olefin selectivity. Deactivation rates decrease and the contribution of active species is larger. This could be explained by an increased diffusion of methanol into the catalyst particles, giving rise to a higher amount of total species in the spent catalyst.

When the diluent is changed from only helium to helium + water (at different ratios) the effect of water is observed. In contrary to literature, water has no influence on the product selectivity and no clear effect on the active period or total reaction time. However, the contribution of active species increase and the total olefin yield increase as well. The amount of deactivated species present in the spent catalysts was slightly increasing for all methanol / water ratios. Using NNMF analysis, it became clear that water influences the reactivity of the reagent / product feed. This is confirmed using propylene feeding experiments with and without extra water. This retardation of reactivity explains a decreased rate of formation for deactivating species and the higher olefin yield as stated before. Since the total amount of deactivated species is almost identical, it can be assumed H-SAPO-34, at these conditions, performs optimal. The decreased formation of active species, the higher contribution of these species at their maximum and the increased IP show that water has competitive adsorption with reagents / products feed. To elaborate on earlier research which focus on the “addition of water”, Figure 39 shows or 14 % Me (Me / Wa = 1/0) and 2 % Me (Me / Wa = 1/6) performance results. To conclude, the addition of water should be separated in adding a diluent, and changing the nature of diluent. It became clear both have their own effect on the MTO process and should be handled with more care since the MTO process and waters reactivity are complex entities influenced by many factors on different scales.

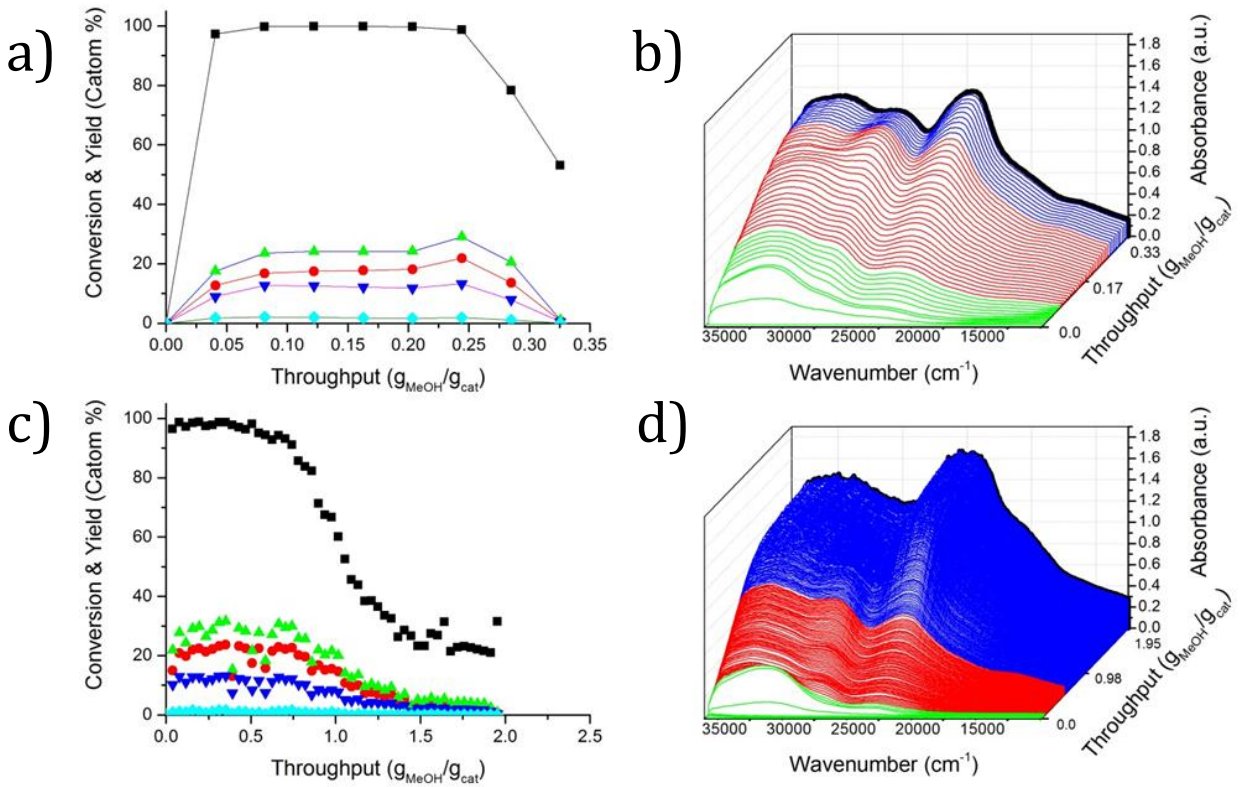

Figure 43. The above conversion and selectivities plots and UV-Vis a & b results show high concentration without water, c & d two show low concentration with Me/Wa = 1/6. This can be considered as "addition of water" as observed in literature. However, the underlying theory is far more complex than stating all observation are due to water.

Chapter 5 – Outlook

This research leaves room for several additional experiments to add to the validity and strength of this work. Although TGA analysis was used for the water experiments, it would be an addition to the concentration results if TGA confirms the huge increase in coke. However, the UV-Vis difference is so large, this would be no necessary addition.

To elucidate on the nature of active species and especially the change when adding water, HF-dissolution experiments could be done as described by Wondergem. [110] These experiments were planned but cancelled due to a lack of time. First of all, the HF dissolution experiments will show what species of cokes are present after the different reactions. This could elucidate on the shift in intensity for the monoenylic → phenanthrene/anthracene carbocations bands as active species for the increased water ratios. Secondly, the difference in active species (methylated naphthalene carbocations instead of HMB carbocations) observed in the propylene feeding experiments could be confirmed. Last, it would be promising to quench the different Me/Wa reactions and perform the HF dissolution, so a glance at what specific active species are acting as co-catalyst could be obtained.

Another addition would be repeating the experiments under other conditions. In this work, concentration tests were performed under two different space velocities, while all water experiments were done under the highest space velocity possible using the given setup. However, a new setup might increase the workable conditions. A higher space velocity has shown the emphasize effects on catalytic performance and therefore results might become more reliable, and if in line with these another argument for given assumptions. When speaking about a new setup, it would be an interesting feature to use larger amounts of catalyst and several UV-Vis probes, focusing on different heights of the catalyst bed. This will give more information about larger scale processes like diffusion, and would be a nice step between small scale (50 mg) to industrial scale.

Although water might behave in similar manner for different catalysts, the amount of acid sites, acid strength and hydrophobicity of the zeolite material might influence the effect of water. Therefore it would be nice to repeat given experiments with different Si / Al ratios, for different types of catalysts and even different materials (SiO_2, Al_2O_3) to create a complete image of the nature of water. However, as became clear during working on this project, the effect of water is complex and not solely to be explained by one given feature.

Maybe the most promising addition would be to do a similar series of experiments but probing with operando IR spectroscopy. Using this technique would allow the imaging of acid sites during the reaction, and could confirm once more that the Brønsted acid sites are influenced by water (by competitive adsorption).

Finally, and as for all research, it would be favorable to repeat the experiments as often as possible and use statistical tests to give the most accurate and significant answers, for example on the slight increase of coke from the TGA analysis.

Chapter 6 – Acknowledgements

During this Master Thesis, I was able to work with a lot of people who learned me skills, helped me with my experiments or contributed in another way. First of all, I would like to thank Javier Ruiz-Martinez. It is quite standard to thank your first supervisor first, but Javier earns more respect. He has taught me to be patient, observational and obtain maximal information from results sometimes seemingly useless. Besides these skills, he was always prepared to answer my questions or open to discussion, even when he left the University and started on a new job. Because of this, I was able to finish my thesis without too much complications, since he could also have let go of my project therefore complicating things in the final stages of my thesis.

Second, I would like to thanks prof. dr. ir. Bert Weckhuysen and dr. Pieter Bruijnincx for being my supervisors and the possibility to do my Master Thesis on the Inorganic Chemistry and Catalysis group. I would also like to thank the group itself and its amazing people for all the nice times, and specifically Remco Dalebout and Koen Bossers for all the good times and fruitful discussions about our projects. Although he was not my daily supervisor, I have to thanks Joris Goetze for daily support, teaching me to work with the operando-setup and always being prepared to answer my questions and help where possible.

At last, I would like to thank my family. First, my girlfriend, Lisanne, for supporting me and giving me feedback on my presentations and written work. Finally, I would like to give credit to my granddad. He passed away on the day of my Thesis final presentation. In the last period of his live he repeatedly mentioned how proud he was of his family and that I should always work hard to achieve my goals.

Chapter 7 – Bibliography

[1] U. Olsbye, S. Svelle, M. Bjørgen, P. Beato, T. V. W. Janssens, F. Joensen, S. Bordiga, and K. P. Lillerud, "Conversion of methanol to hydrocarbons: How zeolite cavity and pore size controls product selectivity," *Angew. Chemie - Int. Ed.*, vol. 51, no. 24, pp. 5810–5831, Jun. 2012.

[2] X. Wu, M. G. Abraha, and R. G. Anthony, "Methanol conversion on SAPO-34: Reaction condition for fixed-bed reactor," *Appl. Catal. A Gen.*, vol. 260, no. 1, pp. 63–69, Mar. 2004.

[3] G. Froment, W. Dehertog, and A. Marchi, "Zeolite catalysis in the conversion of methanol into olefins," *… Chem. Londen, pp. 1-64, …*, 1992.

[4] C. D. Chang, "Hydrocarbons from Methanol," *Catalysis Reviews*, vol. 25. pp. 1–118, 1983.

[5] M. Westgård Erichsen, S. Svelle, and U. Olsbye, "The influence of catalyst acid strength on the methanol to hydrocarbons (MTH) reaction," in *Catalysis Today*, 2013, vol. 215, pp. 216–223.

[6] S. Teketel, U. Olsbye, K. P. Lillerud, P. Beato, and S. Svelle, "Selectivity control through fundamental mechanistic insight in the conversion of methanol to hydrocarbons over zeolites," *Microporous Mesoporous Mater.*, vol. 136, pp. 33–41, 2010.

[7] A. Corma and H. Garcia, "Carbocations and organic radical cations inside zeolite matrices . Generation , characterization , stability and properties," *Top. Catal.*, vol. 6, pp. 127–140, 1998.

[8] S. M. Csicsery, "Shape-selective catalysis in zeolites," in *Zeolites*, 1984, vol. 4, no. 3, pp. 202–213.

[9] S. Ashtekar, S. V. V Chilukuri, and D. K. Chakrabarty, "Small-Pore Molecular Sieves SAPO-34 and SAPO-44 with Chabazite Structure:," pp. 4878–4883, 1994.

[10] K. Hemelsoet, Q. Qian, T. De Meyer, K. De Wispelaere, B. De Sterck, B. M. Weckhuysen, M. Waroquier, and V. Van Speybroeck, "Identification of intermediates in zeolite-catalyzed reactions by in situ UV/Vis microspectroscopy and a complementary set of molecular simulations," *Chem. - A Eur. J.*, vol. 19, no. 49, pp. 16595–16606, Dec. 2013.

[11] F. Bleken, M. Bjørgen, L. Palumbo, S. Bordiga, S. Svelle, K. P. Lillerud, and U. Olsbye, "The effect of acid strength on the conversion of methanol to olefins over acidic microporous catalysts with the CHA topology," *Top. Catal.*, vol. 52, pp. 218–228, 2009.

[12] M. Stöcker, "Methanol-to-hydrocarbons: catalytic materials and their behavior," *Microporous and Mesoporous Materials*, vol. 29. pp. 3–48, 1999.

[13] L.-T. Yuen, S. I. Zones, T. V. Harris, E. J. Gallegos, and A. Auroux, "Product selectivity in methanol to hydrocarbon conversion for isostructural compositions of AFI and CHA molecular sieves," *Microporous Materials*, vol. 2. pp. 105–117, 1994.

[14] C. Marcilly, "Where and how shape selectivity of molecular sieves operates in refining and petrochemistry catalytic processes," *Top. Catal.*, vol. 13, pp. 357–366, 2000.

[15] "IZA Structure Commission." [Online]. Available: www.iza-structure.org.

[16] J. F. Haw, W. Song, D. M. Marcus, and J. B. Nicholas, "The Mechanism of Methanol to Hydrocarbon Catalysis Secondary Reactions : Acid Strength and," vol. 36, no. 5, pp. 317–326, 2003.

[17] Z. Li, J. Martínez-Triguero, P. Concepción, J. Yu, and A. Corma, "Methanol to olefins: activity and stability of nanosized SAPO-34 molecular sieves and control of selectivity by silicon distribution.," *Phys. Chem. Chem. Phys.*, vol. 15, no. 35, pp. 14670–80, Sep. 2013.

[18] D. Mores, E. Stavitski, M. H. F. Kox, J. Kornatowski, U. Olsbye, and B. M. Weckhuysen, "Space- and time-resolved in-situ spectroscopy on the coke formation in molecular sieves: methanol-to-olefin conversion over H-ZSM-5 and H-SAPO-34.," *Chemistry*, vol. 14, no. 36, pp. 11320–7, Jan. 2008.

[19] A. T. Aguayo, A. G. Gayubo, R. Vivanco, M. Olazar, and J. Bilbao, "Role of acidity and microporous structure in alternative catalysts for the transformation of methanol into olefins," *Appl. Catal. A Gen.*, vol. 283, no. 1–2, pp. 197–207, Apr. 2005.

[20] W. Song, D. M. Marcus, H. Fu, J. O. Ehresmann, and J. F. Haw, "An oft-studied reaction that may never have been: Direct catalytic

conversion of methanol or dimethyl ether to hydrocarbons on the solid acids HZSM-5 or HSAPO-34," *J. Am. Chem. Soc.*, vol. 124, pp. 3844–3845, 2002.

[21] C. D. Chang and A. J. Silvestri, "The conversion of methanol and other O-compounds to hydrocarbons over zeolite catalysts," *J. Catal.*, vol. 47, pp. 249–259, 1977.

[22] C. D. Chang, "A Reply to Kagi : Mechanism of Conversion Catalyst of Methanol over ZSM-5," vol. 245, pp. 244–245, 1981.

[23] T. Faradau, E. A. Swabb, and B. C. Gates, "Diffusion, Reaction, and Fouling in H-Mordenite Crystallites. The Catalytic Dehydration of Methanol," vol. 535, no. 1963, pp. 0–5, 1971.

[24] Y. Ono and T. Mori, "Mechanism of methanol conversion into hydrocarbons over ZSM-5 zeolite," *Journal of the Chemical Society, Faraday Transactions 1*, vol. 77. p. 2209, 1981.

[25] D. Kagi, "In Re : Mechanism p * i CH ;.' = ... H ' I," vol. 243, pp. 242–243, 1981.

[26] G. A. Olah, "Higher Coordinate (Hypercarbon Containing) Carbocations and," vol. 53, pp. 201–207, 1981.

[27] C. Engelen, J. Wolthuizen, and J. van Hooff, "On the mechanism of C?C bond formation from methanol over H-ZSM 5. New evidence for trimethyloxonium ion intermediacy," *Journal of the Chemical Society, Chemical Communications*. p. 300, 1985.

[28] J. P. Wolthuizen, J. P. van den Berg, and J. H. C. van Hooff, "Low Temperature Reactions of Olefins on Partially Hydrated Zeolite H-ZSM-5," *Stud. Surf. Sci. Catal.*, vol. 5, pp. 85–92, 1980.

[29] G. J. Hutchings, F. Gottschalk, M. V. M. Hall, and R. Hunter, "Hydrocarbon formation from methylating agents over the zeolite catalyst ZSM-5. Comments on the mechanism of carbon?carbon bond and methane formation," *Journal of the Chemical Society, Faraday Transactions 1*, vol. 83. p. 571, 1987.

[30] W. Zatorski and S. Kryzanowski, "No Title," *Acta Phys. Chem.*, vol. 29, p. 347, 1978.

[31] J. K. A. Clarke, R. Darcy, B. F. Hegarty, E. O'Donoghue, V. Amir-Ebrahimi, and J. J. Rooney, "Free radicals in dimethyl ether on H-ZSM-5 zeolite. A novel dimension of heterogeneous catalysis," *Journal of the Chemical Society, Chemical Communications*. p. 425, 1986.

[32] J. Sauer, M. Sierka, and F. Haase, "Acidic Catalysis by Zeolites: Ab Initio Modeling of Transition Structures," in *Transition State Modeling for Catalysis*, vol. 721, American Chemical Society, 1999, pp. 28–358.

[33] D. Lesthaeghe, V. Van Speybroeck, G. B. Marin, and M. Waroquier, "Understanding the failure of direct C-C coupling in the zeolite-catalyzed methanol-to-olefin process," *Angew. Chemie - Int. Ed.*, vol. 45, pp. 1714–1719, 2006.

[34] D. Lesthaeghe, V. Van Speybroeck, G. B. Marin, and M. Waroquier, "The rise and fall of direct mechanisms in methanol-to-olefin catalysis: An overview of theoretical contributions," in *Industrial and Engineering Chemistry Research*, 2007, vol. 46, pp. 8832–8838.

[35] S. R. Blaszkowski and R. A. Van Santen, "Density functional theory calculations of the activation of methanol by a Brønsted zeolitic proton," *J. Phys. Chem.*, vol. 99, pp. 11728–11738, 1995.

[36] S. R. Blaszkowski, M. A. C. Nascimento, and R. A. van Santen, "Activation of C–H and C–C Bonds by an Acidic Zeolite: A Density Functional Study," *J. Phys. Chem.*, vol. 100, pp. 3463–3472, 1996.

[37] E. Munson and J. Haw, "NMR observation of trimethyloxonium formation from dimethyl ether on zeolite HZSM-5," *J. Am. Chem. Soc.*, no. c, pp. 6303–6305, 1991.

[38] E. J. Munson, A. a. Kheir, and J. F. Haw, "An in situ solid-state NMR study of the formation and reactivity of trialkylonium ions in zeolites," *J. Phys. Chem.*, vol. 97, no. 28, pp. 7321–7327, Jul. 1993.

[39] D. K. Murray, J. W. Chang, and J. F. Haw, "Conversion of methyl halides to hydrocarbons on basic zeolites: a discovery by in situ NMR," *J. Am. Chem. Soc.*, vol. 115, pp. 4732–4741, 1993.

[40] T. R. Forester and R. F. Howe, "In situ FTIR studies of methanol and dimethyl ether in ZSM-5," *J. Am. Chem. Soc.*, vol. 109, pp. 5076–5082, 1987.

[41] W. Wang, A. Buchholz, M. Seiler, and M. Hunger, "Evidence for an Initiation of the Methanol-to-Olefin Process by Reactive

Surface Methoxy Groups on Acidic Zeolite Catalysts," *J. Am. Chem. Soc.*, vol. 125, no. 49, pp. 15260–15267, 2003.

[42] A. Comas-vives, M. Valla, and P. Sautet, "Cooperativity between Al Sites Promotes Hydrogen Transfer and Carbon – Carbon Bond Formation upon Dimethyl Ether Activation on Alumina," 2015.

[43] Q. Zhu, J. N. Kondo, R. Ohnuma, Y. Kubota, M. Yamaguchi, and T. Tatsumi, "The study of methanol-to-olefin over proton type aluminosilicate CHA zeolites," *Microporous Mesoporous Mater.*, vol. 112, no. 1–3, pp. 153–161, Jul. 2008.

[44] A. Izadbakhsh, F. Farhadi, F. Khorasheh, S. Sahebdelfar, M. Asadi, and Y. Z. Feng, "Effect of SAPO-34's composition on its physico-chemical properties and deactivation in MTO process," *Appl. Catal. A Gen.*, vol. 364, no. 1–2, pp. 48–56, Jul. 2009.

[45] R. M. Dessau and R. B. LaPierre, "On the Mechanism of Methanol Conversion over HZSM-5 to Hydrocarbons," vol. 141, pp. 136–141, 1982.

[46] R. M. Dessau, "On the H-ZSM-5 catalyzed formation of ethylene from methanol or higher olefins," *J. Catal.*, vol. 99, pp. 111–116, 1986.

[47] T. Mole, J. A. Whiteside, and D. Seddon, "Aromatic Co-Catalysis of Methanol Conversion over Zeolite Catalysts," *J. Catal.*, vol. 82, pp. 261–266, 1983.

[48] T. Mole, "Conversion of methanol to hydrocarbons over ZSM-5 zeolite: An examination of the role of aromatic hydrocarbons using 13carbon- and deuterium-labeled feeds," *J. Catal.*, vol. 84, pp. 435–445, 1983.

[49] B. E. Langner, "Reactions of methanol on zeolites with different pore structures," *Applied Catalysis*, vol. 2. pp. 289–302, 1982.

[50] I. M. Dahl, "On the Reaction Mechanism for Hydrocarbon Formation from Methanol over SAPO-34 2. Isotopic Labeling Studies of the Co-reaction of Propene and Methanol," *J. Catal.*, vol. 161, no. 1, pp. 304–309, 1996.

[51] I. Dahl and S. Kolboe, "On the Reaction Mechanism for Hydrocarbon Formation from Methanol over SAPO-34," *J. Catal.*, vol. 149, pp. 458–464, 1994.

[52] I. M. Dahl and S. Kolboe, "On the reaction mechanism for propene formation in the MTO reaction over SAPO-34," *Catal. Letters*, vol. 20, pp. 329–336, 1993.

[53] S. Kolboe and I. M. Dahl, *Catalysis by Microporous Materials, Proceedings of ZEOCAT '95*, vol. 94. Elsevier, 1995.

[54] B. Arstad and S. Kolboe, "Methanol-to-hydrocarbons reaction over SAPO-34. Molecules confined in the catalyst cavities at short time on stream," *Catal. Letters*, vol. 71, pp. 209–212, 2001.

[55] B. Arstad and S. Kolboe, "The Reactivity of Molecules Trapped within the SAPO-34 Cavities in the Methanol-to-Hydrocarbons Reaction," no. 58, pp. 8137–8138, 2001.

[56] W. Song, H. Fu, and J. F. Haw, "Supramolecular origins of product selectivity for methanol-to-olefin catalysis on HSAPO-34," *J. Am. Chem. Soc.*, vol. 123, pp. 4749–4754, 2001.

[57] H. Fu, W. Song, and J. F. Haw, "Polycyclic aromatics formation in HSAPO-34 during methanol-to-olefin catalysis: Ex situ characterization after cryogenic grinding," *Catal. Letters*, vol. 76, pp. 89–94, 2001.

[58] W. Song, H. Fu, and J. F. Haw, "Selective synthesis of methylnaphthalenes in HSAPO-34 cages and their function as reaction centers in methanol-to-olefin catalysis," *J. Phys. Chem. B*, vol. 105, pp. 12839–12843, 2001.

[59] J. F. Haw, J. B. Nicholas, W. Song, F. Deng, Z. Wang, T. Xu, and C. S. Heneghan, "Roles for cyclopentenyl cations in the synthesis of hydrocarbons from methanol on zeolite catalyst HZSM-5," *J. Am. Chem. Soc.*, vol. 122, pp. 4763–4775, 2000.

[60] Ø. Mikkelsen, P. O. Rønning, and S. Kolboe, "Use of isotopic labeling for mechanistic studies of the methanol-to-hydrocarbons reaction. Methylation of toluene with methanol over H-ZSM-5, H-mordenite and H-beta," *Microporous Mesoporous Mater.*, vol. 40, pp. 95–113, 2000.

[61] M. Bjørgen, U. Olsbye, and S. Kolboe, "Coke precursor formation and zeolite deactivation: Mechanistic insights from hexamethylbenzene conversion," *J. Catal.*, vol. 215, pp. 30–44, 2003.

[62] M. Bjørgen, F. Bonino, S. Kolboe, K. P. Lillerud, A. Zecchina, and S. Bordiga, "Spectroscopic Evidence for a Persistent Benzenium Cation in Zeolite H-Beta," *J. Am. Chem. Soc.*, vol. 125, pp. 15863–15868, 2003.

[63] M. Bjørgen, U. Olsbye, D. Petersen, and S. Kolboe, "The methanol-to-hydrocarbons reaction: Insight into the reaction mechanism from [12C]benzene and [13C]methanol coreactions over zeolite H-beta," *J. Catal.*, vol. 221, pp. 1–10, 2004.

[64] M. Bjørgen, U. Olsbye, S. Svelle, and S. Kolboe, "Conversion of methanol to hydrocarbons : the reactions of the hepta-methylbenzenium cation over zeolite H-beta," vol. 93, no. March, pp. 37–40, 2004.

[65] J. Haw, D. Marcus, and P. Kletnieks, "Comments on 'Effect of organic impurities on the hydrocarbon formation via the decomposition of surface methoxy groups on acidic zeolite catalysts' by Y. Jiang, W. Wang, V.R.R. Marthala, J. Huang, B. Sulikowski, M. Hunger," *J. Catal.*, vol. 244, no. 1, pp. 130–133, Nov. 2006.

[66] C. Vogt, "Combined In-situ Spectroscopy Techniques to Investigate the Effect of Gas Phase Impurities and Regeneration on the MTO Process," 2014.

[67] C. J. Egaii, R. P. Sieg, G. E. Langlois, and R. F. Sullivan, "A New Reaction That Occurs in the Hydrocracking of Certain Aromatic Hydrocarbons," *J. Am. Chem. Soc.*, vol. 83, pp. 1156–1160, 1961.

[68] S. Svelle, M. Bjørgen, S. Kolboe, D. Kuck, M. Letzel, U. Olsbye, O. Sekiguchi, and E. Uggerud, "Intermediates in the Methanol-to-hydrocarbons (MTH) Reaction: A Gas Phase Study of the Unimolecular Reactivity of Multiply Methylated Benzenium Cations," *Catal. Letters*, vol. 109, no. 1–2, pp. 25–35, Jun. 2006.

[69] O. Sekiguchi, V. Mayer, M. C. Letzel, D. Kuck, and E. Uggerud, "Energetics and reaction mechanisms for the competitive losses of H2, CH4 and C2H4 from protonated methylbenzenes--implications to the methanol- to-hydrocarbons (MTH) process.," *Eur. J. Mass Spectrom. (Chichester, Eng).*, vol. 15, pp. 167–181, 2009.

[70] C. M. Wang, Y. D. Wang, H. X. Liu, Z. K. Xie, and Z. P. Liu, "Theoretical insight into the minor role of paring mechanism in the methanol-to-olefins conversion within HSAPO-34 catalyst," *Microporous Mesoporous Mater.*, vol. 158, pp. 264–271, 2012.

[71] C.-M. Wang, Y.-D. Wang, Z.-K. Xie, and Z.-P. Liu, "Methanol to Olefin Conversion on HSAPO-34 Zeolite from Periodic Density Functional Theory Calculations: A Complete Cycle of Side Chain Hydrocarbon Pool Mechanism," *J. Phys. Chem. C*, vol. 113, no. 11, pp. 4584–4591, Mar. 2009.

[72] K. De Wispelaere, K. Hemelsoet, M. Waroquier, and V. Van Speybroeck, "Complete low-barrier side-chain route for olefin formation during methanol conversion in H-SAPO-34," *J. Catal.*, vol. 305, pp. 76–80, Sep. 2013.

[73] C.-M. Wang, Y.-D. Wang, H.-X. Liu, Z.-K. Xie, and Z.-P. Liu, "Catalytic activity and selectivity of methylbenzenes in HSAPO-34 catalyst for the methanol-to-olefins conversion from first principles," *J. Catal.*, vol. 271, no. 2, pp. 386–391, May 2010.

[74] A. Sassi, M. A. Wildman, H. J. Ahn, P. Prasad, J. B. Nicholas, and J. F. Haw, "Methylbenzene chemistry on zeolite HBeta: Multiple insights into methanol-to-olefin catalysis," *J. Phys. Chem. B*, vol. 106, pp. 2294–2303, 2002.

[75] A. Sassi, M. A. Wildman, and J. F. Haw, "Reactions of butylbenzene isomers on zeolite Hbeta: Methanol-to-olefins hydrocarbon pool chemistry and secondary reactions of olefins," *J. Phys. Chem. B*, vol. 106, pp. 8768–8773, 2002.

[76] U. Olsbye, M. Bjørgen, S. Svelle, K. P. Lillerud, and S. Kolboe, "Mechanistic insight into the methanol-to-hydrocarbons reaction," in *Catalysis Today*, 2005, vol. 106, pp. 108–111.

[77] E. Borodina, F. Meirer, I. Lezcano-Gonzalez, M. Mokhtar, A. M. Asiri, S. A. Al-Thabaiti, S. N. Basahel, J. Ruiz-Martinez, and B. M. Weckhuysen, "Influence of the Reaction Temperature on the Nature of the Active and Deactivating Species during Methanol-to-Olefins Conversion over H SSZ 13," *ACS Catal.*, vol. 5, pp. 992–1003, Dec. 2015.

[78] J. W. Park, J. Y. Lee, K. S. Kim, S. B. Hong, and G. Seo, "Effects of cage shape and size of 8-membered ring molecular sieves on their deactivation in methanol-to-olefin (MTO) reactions," *Appl. Catal. A Gen.*, vol. 339, no. 1, pp. 36–44, Apr. 2008.

[79] K. Hemelsoet, A. Nollet, V. Van Speybroeck, and M. Waroquier, "Theoretical simulations elucidate the role of naphthalenic species during methanol conversion within H-SAPO-34.," *Chem. - A Eur. J.*, vol. 17, no. 33, pp. 9083–93, Aug. 2011.

[80] B. Azambre, a. Westermann, G. Finqueneisel, F. Can, and J. D. Comparot, "Adsorption and Desorption of a Model Hydrocarbon Mixture Over HY Zeolite Under Dry and Wet Conditions," *J. Phys. Chem. C*, vol. 119, no. 1, pp. 315–331, 2015.

[81] N. Mo and P. E. Savage, "Hydrothermal Catalytic Cracking of Fatty Acids with HZSM‐5," 2013.

[82] a. S. M. Junaid, M. M. Rahman, G. Rocha, W. Wang, T. Kuznicki, W. C. McCaffrey, and S. M. Kuznicki, "On the role of water in natural-zeolite-catalyzed cracking of athabasca oilsands bitumen," *Energy and Fuels*, vol. 28, no. 5, pp. 3367–3376, 2014.

[83] K. D. Dubois, C. Liu, and G. Li, "Involvement of surface-adsorbed water in photochromism of spiropyran molecules deposited on NaY zeolite," *Chem. Phys. Lett.*, vol. 598, pp. 53–57, 2014.

[84] H.-S. Jang, K. Bae, M. Shin, S. M. Kim, C.-U. Kim, and Y.-W. Suh, "Aromatization of glycerol/alcohol mixtures over zeolite H-ZSM-5," *Fuel*, vol. 134, no. 2014, pp. 439–447, 2014.

[85] K. Chen, J. Damron, C. Pearson, D. Resasco, L. Zhang, and J. L. White, "Zeolite Catalysis: Water Can Dramatically Increase or Suppress Alkane C–H Bond Activation," *ACS Catal.*, pp. 3039–3044, 2014.

[86] Y. Xu, C. P. Grey, J. M. Thomas, and A. K. Cheetham, "An Investigation into the conversion of methanol to hydrocarbons over a SAPO-34 catalyst using Magic-Angle-Spinning NMR and Gas Chromatography," *Catal. Letters*, vol. 4, pp. 251–260, 1990.

[87] W. J. H. Dehertog and G. F. Froment, "Production of light alkenes from methanol on ZSM-5 catalysts," *Appl. Catal.*, vol. 71, no. 1, pp. 153–165, 1991.

[88] M. J. Van Niekerk, J. C. Q. Fletcher, and C. T. O. Connor, "Effect of catalyst modification on the conversion of methanol to light olefins over SAPO-34," *Appl. Catal.*, vol. 138, pp. 135–145, 1996.

[89] X. Wu and R. G. Anthony, "Effect of feed composition on methanol conversion to light olefins over SAPO-34," *Appl. Catal. A Gen.*, vol. 218, no. 1–2, pp. 241–250, 2001.

[90] M. Shahda, Y. Dengchao, and W. Huixin, "Methanol Conversion to Hydrocarbons over a SAPO-34 Catalyst in a Pulse Micro Reactor," *Pet. Sci. Technol.*, vol. 26, no. 16, pp. 1893–1903, 2008.

[91] A. Taheri Najafabadi, S. Fatemi, M. Sohrabi, and M. Salmasi, "Kinetic modeling and optimization of the operating condition of mto process on sapo-34 catalyst," *J. Ind. Eng. Chem.*, vol. 18, no. 1, pp. 29–37, 2012.

[92] M. J. Truitt, S. S. Toporek, R. Rovira-Truitt, and J. L. White, "Alkane C-H bond activation in zeolites: Evidence for direct protium exchange," *J. Am. Chem. Soc.*, vol. 128, no. 6, pp. 1847–1852, 2006.

[93] M. J. Truitt, S. S. Toporek, R. Rovira-Hernandez, K. Hatcher, and J. L. White, "Identification of an adsorption complex between an alkane and zeolite active sites," *J. Am. Chem. Soc.*, vol. 126, no. 36, pp. 11144–11145, 2004.

[94] K. Chen, J. Damron, C. Pearson, D. Resasco, L. Zhang, and J. L. White, "Zeolite Catalysis: Water Can Dramatically Increase or Suppress Alkane C–H Bond Activation," *ACS Catal.*, pp. 3039–3044, 2014.

[95] T. Okuhara, "Water-tolerant solid acid catalysts," *Chem. Rev.*, vol. 102, no. 10, pp. 3641–3666, 2002.

[96] D. D. Hibbitts, B. T. Loveless, M. Neurock, and E. Iglesia, "Mechanistic role of water on the rate and selectivity of fischer-tropsch synthesis on ruthenium catalysts," *Angew. Chemie - Int. Ed.*, vol. 52, no. 47, pp. 12273–12278, 2013.

[97] S. Bordiga, L. Regli, D. Cocina, C. Lamberti, M. Bjørgen, and K. P. Lillerud, "Assessing the acidity of high silica chabazite H-SSZ-13 by FTIR using CO as molecular probe: Comparison with H-SAPO-34," *J. Phys. Chem. B*, vol. 109, no. 7, pp. 2779–2784, 2005.

[98] R. Schachtner, G. Poeppel, A. M. Tomé, and E. W. Lang, "A Bayesian approach to the Lee-Seung update rules for NMF," *Pattern Recognit. Lett.*, vol. 45, pp. 251–256, 2014.

[99] E. F. Gonzalez and Y. Zhang, "Accelerating the Lee-Seung algorithm for non-negative matrix factorization," 2005.

[100] I. Lezcano-Gonzalez, U. Deka, B. Arstad, a Van Yperen-De Deyne, K. Hemelsoet, M. Waroquier, V. Van Speybroeck, B. M. Weckhuysen, and a M. Beale, "Determining the storage, availability and reactivity of NH3 within Cu-Chabazite-based Ammonia Selective Catalytic Reduction systems.," *Phys. Chem. Chem. Phys.*, vol. 16, no. 4, pp. 1639–50, 2014.

[101] H. Y. Jeon, C. H. Shin, H. J. Jung, and S. B. Hong, "Catalytic evaluation of small-pore molecular sieves with different framework topologies for the synthesis of methylamines," *Appl. Catal. A Gen.*, vol. 305, no. 1, pp. 70–78, 2006.

[102] Q. Zhu, J. N. Kondo, T. Tatsumi, S. Inagaki, R. Ohnuma, Y. Kubota, Y. Shimodaira, H. Kobayashi, and K. Domen, "A comparative study of methanol to olefin over CHA and MTF zeolites," *J. Phys. Chem. C*, vol. 111, no. 14, pp. 5409–5415, 2007.

[103] G. V. A. Martins, G. Berlier, C. Bisio, S. Coluccia, H. O. Pastore, and L. Marchese, "Quantification of br??nsted acid sites in microporous catalysts by a combined FTIR and NH3-TPD study," *J. Phys. Chem. C*, vol. 112, no. 18, pp. 7193–7200, 2008.

[104] International Zeolite Association, "X-Ray Diffraction Patterns Database of Zeolite Structures," *Framework type code CHA*.

[Online]. Available: http://izasc.biw.kuleuven.be/fmi/xsl/IZA-SC/mat_xrd.xsl?-db=crystal_data&-. [Accessed: 21-Sep-2015].

[105] K. Hemelsoet, A. Ghysels, D. Mores, K. De Wispelaere, V. Van Speybroeck, B. M. Weckhuysen, and M. Waroquier, "Experimental and theoretical IR study of methanol and ethanol conversion over H-SAPO-34," *Catal. Today*, vol. 177, no. 1, pp. 12–24, Nov. 2011.

[106] V. VanSpeybroeck, K. Hemelsoet, K. DeWispelaere, Q. Qian, J. VanderMynsbrugge, B. DeSterck, B. M. Weckhuysen, and M. Waroquier, "Mechanistic Studies on Chabazite-Type Methanol-to-Olefin Catalysts: Insights from Time-Resolved UV/Vis Microspectroscopy Combined with Theoretical Simulations," *ChemCatChem*, vol. 5, no. 1, pp. 173–184, 2013.

[107] W. Dai, M. Scheibe, L. Li, N. Guan, and M. Hunger, "Effect of the methanol-to-olefin conversion on the PFG NMR self-diffusivities of ethane and ethene in large-crystalline SAPO-34," *J. Phys. Chem. C*, vol. 116, no. 3, pp. 2469–2476, 2012.

[108] W. Dai, M. Scheibe, N. Guan, L. Li, and M. Hunger, "Fate of Brønsted Acid Sites and Benzene-Based Carbenium Ions During Methanol-to-Olefin Conversion on SAPO-34," *ChemCatChem*, vol. 3, no. 7, pp. 1130–1133, 2011.

[109] W. Dai, G. Wu, L. Li, N. Guan, and M. Hunger, "Mechanisms of the deactivation of SAPO-34 materials with different crystal sizes applied as MTO catalysts," *ACS Catal.*, vol. 3, no. 4, pp. 588–596, 2013.

[110] K. Wondergem, J. Ruiz-Martinez, and B. M. Weckhuysen, "The Effect of Water on Methanol-to-Olefins Reactions Studied by Advanced in situ Microspectroscopy," 2014.

Appendix A - Calculations

Using Antoine's equation $log10\ p = A - \frac{B}{C+T}$ or $T = \frac{B}{A-log10\ p} - C$ enables to calculate the vapor pressure p given at certain temperature T. The constants A, B & C differ per compound. For methanol, the following constants are used:

***A* = 7.87863, *B* = 1473.11 and *C* = 230.0** (taken from Lange's Handbook of Chemistry, 10th edition).

For water, the following constants are used:

***A* = 8.07131, *B* = 1730.63 and *C* = 233.426** (used for 1 °C < T < 100 °C)

Plotting both formulas with given constants produces the following image:

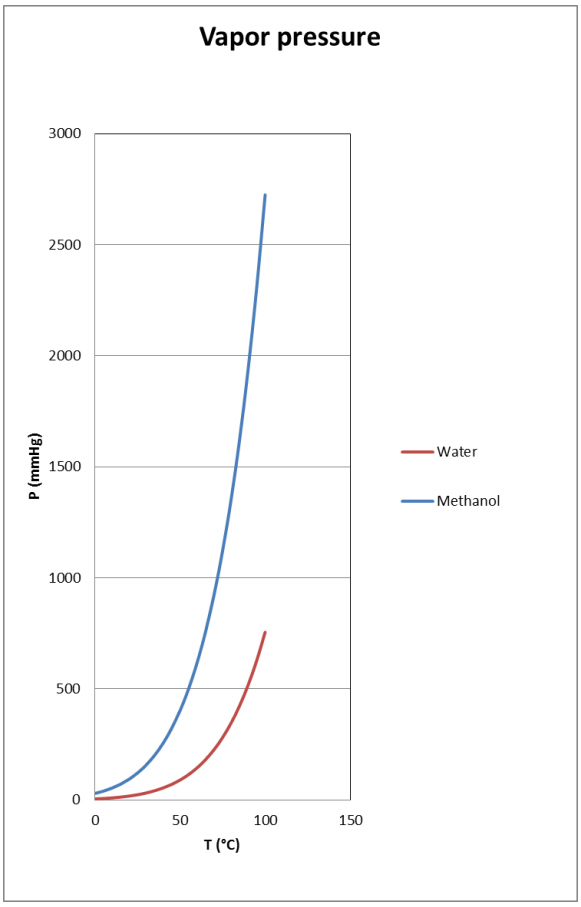

Using T(methanol) = 28 °C and T(water) = 62 °C gives a p = 1.5 * 10^2 which accounts for C = 0.008 mol/L.

To calculate the possibilities for a propylene-feeding experiment on the available setup, several factors needed to be kept in mind. The minimum achievable flow for propylene using the mass flow controller was 2 mL/min. The MFC was calibrated for propane, meaning the gas constants needed to be normalized. The actual flow therefore was $\frac{propylene}{propane} = \frac{0.401}{0.343} = 1.17$ times bigger, so 2 mL/min * 1.17 = 2.34 mL/min propylene. This would account for 0.104 mmol/min (using V_{mol} = 22.5 dm^3/mol, = 22.5 mL/mmol, T = 298 K), equivalent to 0.00437 g/min (using M_{mol} = 42.08 g/mol/0.04208 g/mmol) > 0.2626 g/h > 5.25 g/(g.h) (since 50 mg was used) which means the space velocity is similar to the original $WHSV_{MeOH}$ = 4 g/(g.h).

Pure theoretical, the reaction 3 MeOH → propylene + 3 water contains propylene / water = 1/3. This means the concentration of water should be 0.312 mmol/min. If we use 100 mL/min, this means the temperature used for the saturator should be ~45 °C (c = 0.004 mmol/mL). The stoichiometrical correct experiment should therefore be 2.34 mL/min propylene with 100 mL/min He/H_2O and T_{sat} = 45 °C. However, it is performed with 100 mL/min He/H_2O at 25 °C due to technical problems and a lack of time to redo it, making the propylene / water ratio ≃ 1/1. The propylene + water experiment was performed with 2.34 mL/min propylene with 100 mL/min He/H_2O and T_{sat} = 65 °C (c = 0.009 mmol/mL) representing propylene / water ≃ 1/ 9.

To calculate the amount of silica atoms responsible for Brønsted acid sites, the amount of ammonium is shown to be 0.917 $mmol/g_{cat}$ using 22.4 dm^3/mol and the amount of desorbed ammonia. The total amount of silica is 10% per gram cat (TDS ACS Materials) > 0.1 g SiO_2 > 1.66 $mmol_{Si}/g_{cat}$. (0.917/1.66) * 100% = 55% of the silica atoms.

Appendix B – Additional Figures

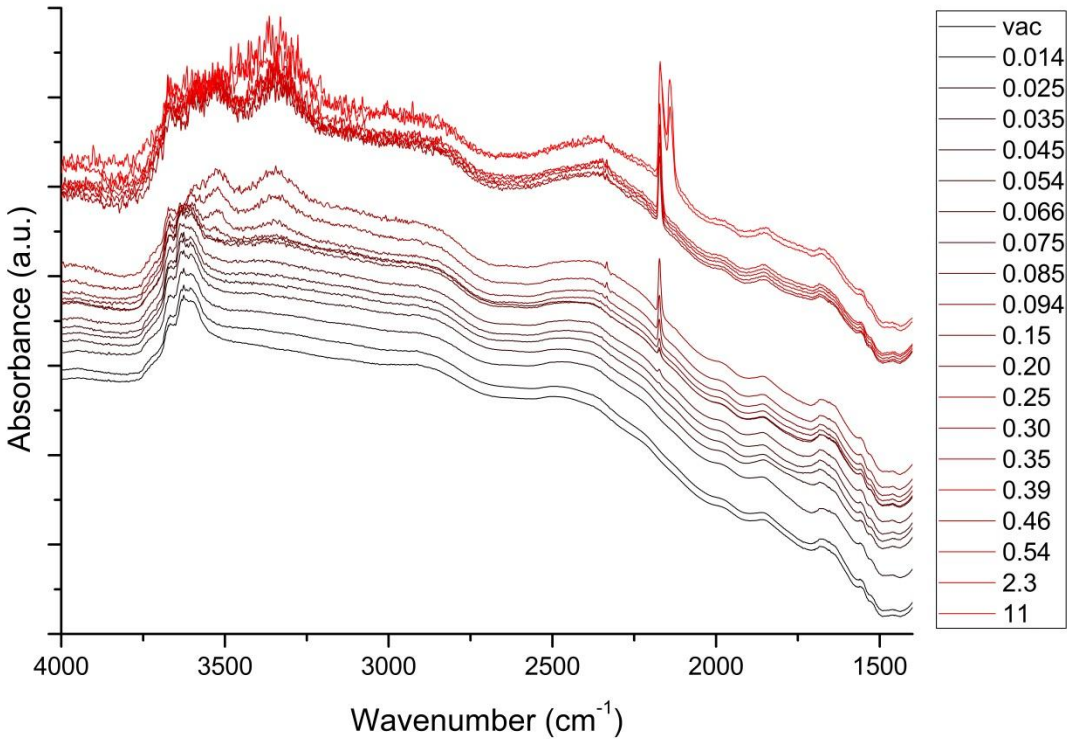

Figure 44. Complete FT-IR measurement for the H-SAPO-34 catalyst.
From black to red shows increasing pressure of CO.

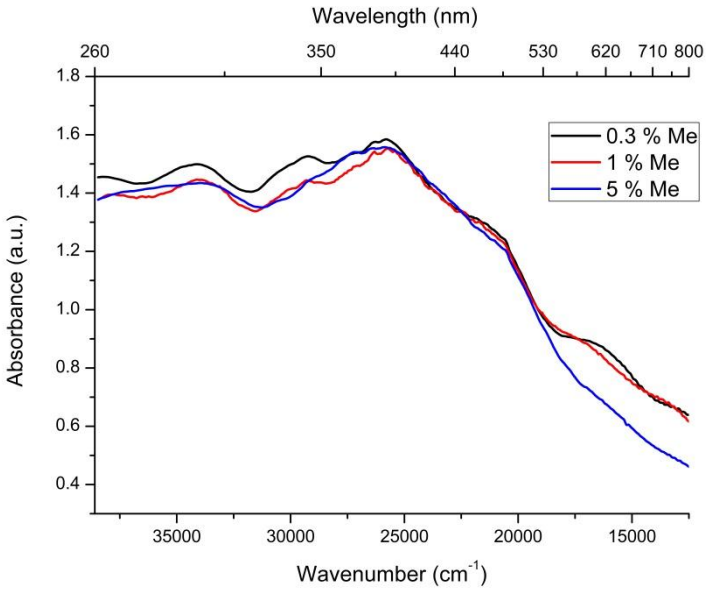

Figure 45. UV-Vis spectra taken from the concentration experiments at WHSV = 0.3 g/(g.h). The taken spectra are the last recorded and therefore account for the species present after catalyst deactivation. The spectra shown here are the black spectra from the corresponding Operando UV-vis figures.

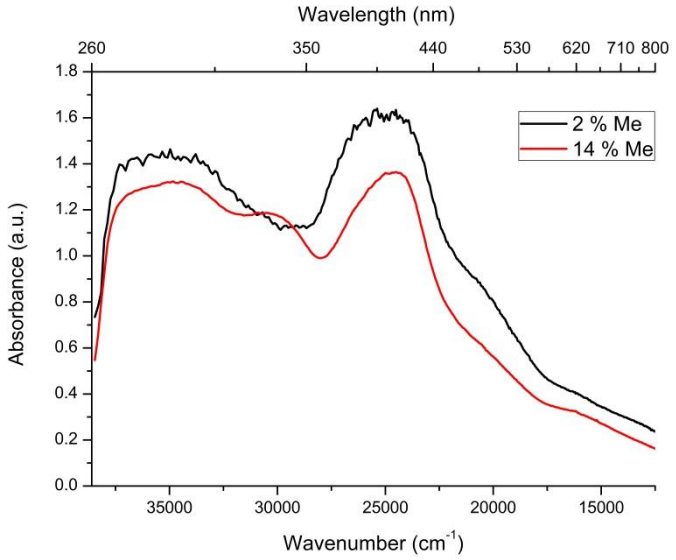

Figure 46. UV-Vis spectra taken from the concentration experiments at WHSV = 4 g/(g.h). The taken spectra are the last recorded and therefore account for the species present after catalyst deactivation. The spectra shown here are the black spectra from the corresponding Operando UV-vis figures.

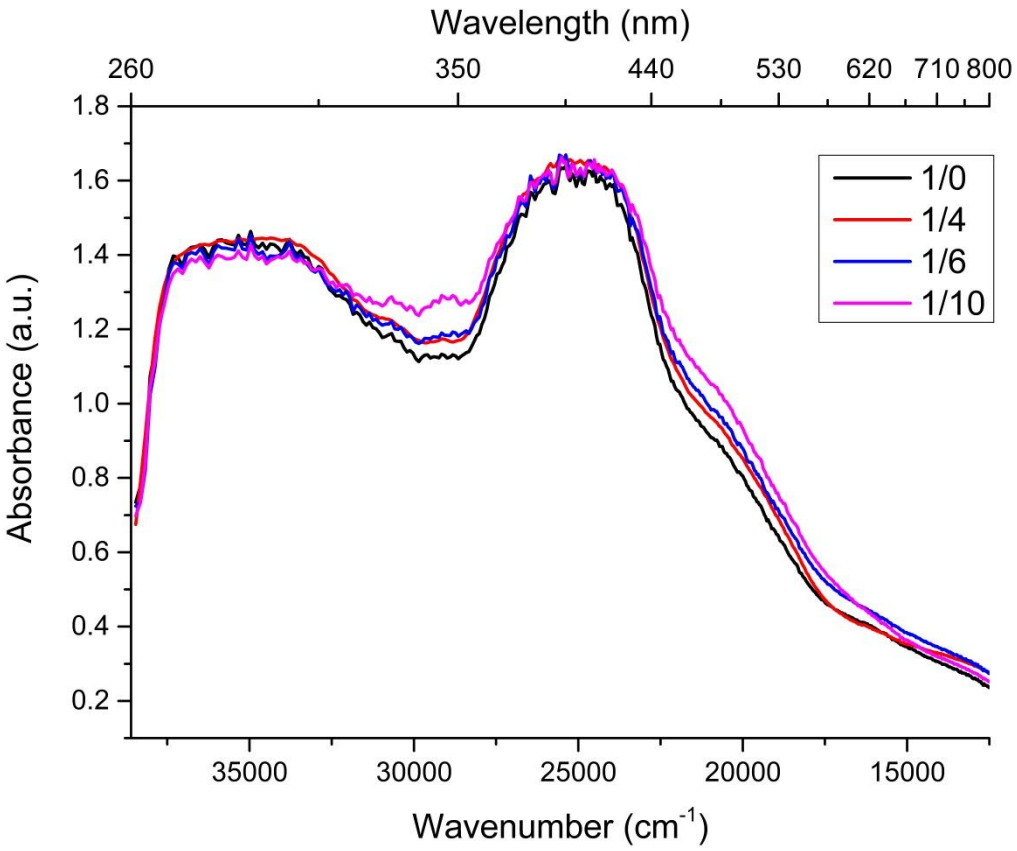

Figure 47. UV-Vis spectra taken from the water experiments at WHSV = 4 g/(g.h), on the H-SAPO-34 catalyst. The taken spectra are the last recorded and therefore account for the species present after catalyst deactivation. The spectra shown here are the black spectra from the corresponding Operando UV-vis figures.